

A New Variational Method with Application to Strongly Correlated Electrons

A dissertation submitted to the
SWISS FEDERAL INSTITUTE OF TECHNOLOGY ZÜRICH

for the degree of
Doctor of Natural Sciences

presented by
ELMAR HEEB
Dipl. Phys. ETH
born December 7, 1964
citizen of Altstätten (SG)

accepted on the recommendation of
Prof. Dr. T. M. Rice, examiner
Prof. Dr. R. J. Joynt, co-examiner

1994

Acknowledgement / Dank

First of all I would like to thank my thesis advisor Prof. T. M. Rice for giving me the opportunity to work in the interesting field of strongly correlated electrons. He initiated this work and throughout the project he helped to move it forward whenever I seemed stuck. In many discussions I learned from him not only about the physics involved but also on how one should approach such a project. Most importantly, he created an atmosphere which makes it a pleasure to work in his group.

I appreciate very much that Prof. R. J. Joynt took on the job of co-referee. This work profited greatly especially in its final stages from the discussions with him. Special thanks go also to his student Benjamin E. C. Koltenbah for his help in cross-checking our programs, a task which is invaluable for any numerical work.

With his continuous support Prof J. W. Blatter provided many helpful insights into the details of research and helped out with all the information that is hard to find in any books.

This work was influenced by many friends and colleagues. S. E. Barnes suggested to combine the Lanczos and the variational Monte Carlo methods which turned out to be a very versatile tool. I am especially thankful to Marco Luchini and Andreas Schönenberger with whom I shared my office. I enjoyed countless discussions with Nick Bonesteel, Beni Braun, Jeff Clayhold, Roland Fehrenbacher, Richard Hlubina, Masao Ogata, Didier Poilblanc, Peter Prelovšek, Bill Putikka, Reto Quadroni, Sandy Rutherford, Manfred Sigrist, Christiane de Morais Smith, Matthias Troyer, and Hirokazu Tsunetsugu. Roland Fehrenbacher deserves a special thank for his help with the details of \TeX .

Zum Gelingen dieser Dissertation haben auch all jene beigetragen, die für einen Ausgleich zur Forschung sorgten. Einen speziellen Dank möchte ich für Thomas Schulthess, Daniel Weiss, Matthias Krieger, Gabriel und Madeleine Schenker sowie für Brigitte Böhi aussprechen.

Während all der Jahre konnte ich stets auf die Unterstützung meiner Eltern und meiner Schwestern Silvia und Gabriela zählen. Sie verdienen meinen innigsten Dank.

Ferner möchte ich die Unterstützung durch den Schweizerischen Nationalfond verdanken.

Kurzfassung

In der vorliegenden Dissertation wird eine neue variationelle Methode vorgestellt, welche die Vorteile der exakten Diagonalisierung nach dem Lanczos Verfahren für kleine Systeme mit der variationellen Monte-Carlo Methode für grosse Systeme verbindet. Da diese neue Methode weder von der Existenz eines kleinen Parameters abhängt noch unter dem Fermionen-Vorzeichenproblem leidet, eignet sie sich gut zur Untersuchung fermionischer Systeme mit starken Korrelationen.

Nach einer kurzen Einführung im ersten Kapitel über ein paar Modelle stark korrelierter Elektronensysteme, welche die Motivation bilden, den neuen Ansatz zu entwickeln, wird die Methode im Detail in Kapitel 2 erklärt. Lanczos Iterationen führen zu einer kontrollierten Verbesserung einer vorurteilsfreien variationellen Wellenfunktion. Eine Verallgemeinerung der Lanczos Operatoren erlaubt es, genauere Resultate mit nur einer Iteration zu erhalten. Dadurch werden die übermässigen Rechenzeiten für die Lanczos-Iterationen höherer Ordnung vermieden. Anstatt mehrere Iterationen auszuführen, kann systematisch eine Hierarchie immer allgemeinerer Lanczos Operatoren konstruiert werden, mit welchen eine Iteration durchgeführt wird. Im Falle des t - J Modells führt dies zu einer getrennten Behandlung der kurz- und langreichweitigen Eigenschaften des Grundzustandes. Mit Hilfe eines kombinierten Kriteriums für die Energie und die Varianz einer variationellen Wellenfunktion vor und nach der Lanczos Iteration, ist es möglich die Qualität des Ansatzes zu überprüfen und dadurch den systematischen Fehler, welche in der Wahl einer variationellen Wellenfunktion besteht, zu einem grossen Teil zu beseitigen. Kapitel 3 diskutiert die Details, welche mit der Implementation des Algorithmus zusammenhängen.

Die Methode wird zuerst am Fall des Heisenberg-Modells in Kapitel 4 getestet. Dieses Modell erlaubt äquivalente Formulierungen in bosonischer oder fermionischer Darstellung. Die neue Methode kann an der fermionischen Formulierung getestet werden, indem man die Resultate mit den zuverlässigen Daten, welche aufgrund der bosonischen Darstellung zur Verfügung stehen, vergleicht. Die neue Methode liefert eine bessere obere Schranke für die Grundzustandsenergie als frühere Rechnungen, welche sich ebenfalls auf die fermionische Darstellung abstützten. Der Vergleich mit Quanten-Monte-Carlo Resultaten für den bosonischen Fall zeigt, dass mit jeder Iteration etwa 80% der noch fehlenden Korrelationsenergie in der neuen Wellenfunktion berücksichtigt wird, sofern der Hilbert-Raum mit der richtigen Symmetrie verwendet wird. Ferner werden Messungen der Spin-Spin-Korrelationsfunktion gezeigt, welche einen guten Wert für die alternierende Magnetisierung liefert.

Im Kapitel 5 werden Berechnungen zum t - J Modell präsentiert, der wichtigsten Anwendung der neuen Methode in dieser Dissertation. Für dieses Modell gibt es keine äquivalente bosonische Darstellung und die Quanten-Monte-Carlo Methoden

sind aufgrund des Vorzeichenproblems für Fermionen nur stark eingeschränkt verwendbar. Mit der neuen Methode, die nicht unter dem Vorzeichenproblem leidet, können die Resultate der exakten Diagonalisierung für kleine Systeme reproduziert werden. Die gleichen Untersuchungen werden dann an einem viel grösseren System durchgeführt, als es mit der exakten Diagonalisierung möglich wäre. Die Messung der Energie und der Varianz zeigt eine gute Konvergenz zum Grundzustand für die gewählten Variationswellenfunktionen. Mittels der Maxwell-Konstruktion erhält man eine Abschätzung für die Phasenseparationsgrenze im Phasendiagramm. Durch die getrennte Behandlung des kurz- und langreichweitigen Verhaltens der Wellenfunktion mittels der verallgemeinerten Lanczos Operatoren, ist es möglich die langreichweitige Paar-Paar-Korrelation des Grundzustandes zu messen. Diese ist ein Mass für den Supraleitungs-Ordnungsparameter und sie erlaubt es eine Region mit d-Wellen-Supraleitungs-Ordnung im $T = 0$ -Phasendiagramm des 2-dimensionalen t - J Modells zu identifizieren.

Die Resultate für das t - J Modell zeigen, dass diese neue Methode der verallgemeinerten Lanczos Operatoren in der Variations-Monte-Carlo Methode ein mächtiges Werkzeug darstellt, um vorurteilsfreie Resultate für ein nicht triviales Quanten-Vielteilchensystem zu erhalten. Daher erwartet man, dass sich die neue Methode auch in anderen Problemen bewähren wird. Dies ist speziell dort zu erwarten, wo Vorzeichenprobleme den Gebrauch der üblichen Quanten-Monte-Carlo Methoden einschränkt.

Abstract

In this thesis a new variational method is presented which combines the advantages of the Lanczos method used in exact diagonalizations of small systems and the variational Monte Carlo method used to investigate large systems. As this new method does not depend on the existence of a small parameter nor is limited by the fermion sign problem it is well suited for the investigation of fermionic systems with strong correlations.

After a short introduction in the first chapter to some models of strongly correlated many electron systems which motivated the development of the new approach, the method is explained in detail in chapter 2. Lanczos iterations can be used to construct an unbiased systematic improvement of a variational wavefunction. A generalization of the Lanczos operators allows one to obtain more accurate results with only one iteration. This avoids the excessive time requirements of higher order Lanczos iterations. Instead of performing many iterations one can systematically construct a hierarchy of ever more general Lanczos operators to be used in a single iteration. For the case of the t - J model this amounts to a separate treatment of the short- and long-range properties of the groundstate. Using a combined criterion of energy and variance of the variational wavefunctions before and after the iteration it is possible to judge the quality of the starting variational wavefunction and thereby eliminate much of the bias which lies in the choice of such a wavefunction. Chapter 3 discusses the details associated with the implementation of the algorithm.

The method is tested first for the Heisenberg model in chapter 4. For this model there are equivalent formulations using boson and fermion representations. It is possible to test the new method for the fermionic formulation by comparing with the reliable results available for the bosonic representation. Our approach leads to a better upper limit to the groundstate energy than previous calculations which also use a fermionic representation. The comparison with Quantum Monte Carlo results for the bosonic case shows that the presented method is able to recover about 80% of the missing correlation energy in each Lanczos iteration when using the right symmetry sector of the Hilbert space. Measurements of the spin-spin correlation which yield a good value for the staggered magnetization are also presented.

In chapter 5 calculations on the t - J model are presented, which constitutes the main application for the new method in this thesis. For this model there is no equivalent bosonic representation and Quantum Monte Carlo methods are severely limited by the fermion sign problem. With the new method, which does not suffer the sign problem, the results of exact diagonalization for small systems can be reproduced. Then the same analysis is performed on a much bigger system than would be possible with the exact methods. The energy and variance are measured, which shows

good convergence to the groundstate for the chosen set of wavefunctions. With a Maxwell construction one finds an estimate for the phase separation boundary in the phase diagram. The separate treatment of the short- and long-range behavior of the wavefunctions using the generalized Lanczos operators makes it possible to measure the long-range pair-pair correlation of the groundstate. This is a measure of the superconducting order parameter and it allows the identification of a region of d-wave superconducting order in the zero temperature phase diagram of the 2 dimensional t - J model.

The results on the t - J model show that this new method of the generalized Lanczos operators in variational Monte Carlo provides a powerful tool to obtain unbiased results for a non-trivial quantum many body system. This suggests that the presented method could be used successfully to address other problems, especially those where the standard Quantum Monte Carlo methods are of limited use due the fermion sign problem.

Contents

1	Models for the Copper Oxide Superconductors	1
1.1	The Three-Band Hubbard Model	2
1.2	The t - J Model	3
1.3	The One-Band Hubbard Model	3
1.4	Some Known Results about the t - J Model	4
1.4.1	Magnetic Order	4
1.4.2	Hole Binding and Phase Separation	5
1.4.3	Superconductivity	6
2	The Method	8
2.1	The Rayleigh-Ritz Principle and Generalizations	8
2.2	Systematic Improvement by Lanczos Iteration	10
2.3	Limitations for Higher Moments and the Sign Problem	11
2.4	Separate Treatment of the Short- and Long-Range Behavior	14
2.5	Non-Variational Results from One Lanczos Iteration	15
2.6	Generalized Lanczos Operators	16
2.7	Wavefunctions	17
2.8	Lattices and Finite Size Effects	18
3	Implementation of the Algorithm	22
3.1	Monte Carlo Sampling	22
3.2	Importance Sampling	23
3.3	Statistical Errors	25
3.4	Determinant Updates	26
3.5	Efficient Reuse of Intermediate Results	28
3.6	Some Implementation Details	29
4	The Heisenberg Model	31
4.1	The Heisenberg Model as a Test Case	32
4.2	Variational Monte Carlo with Lanczos Iterations	33
4.3	Spin Order	37

4.4	Conclusions	39
5	The t-J Model	40
5.1	Energy and Variance	43
5.1.1	Quarter Filling	44
5.1.2	Hole Dopings $\delta = 0.16$ and $\delta = 0.32$	49
5.2	Phase Separation	51
5.3	Superconducting Long-Range Order	53
5.4	The Phase Diagram	59
6	Conclusions	61

Chapter 1

Models for the Copper Oxide Superconductors

Many of the main characteristics of the copper oxide superconductors are consequences of the fact that they are close to a Mott insulator. Typical materials have a “parent” compound which is an antiferromagnetic insulator. Upon doping the antiferromagnetism is quickly suppressed and a superconducting phase appears with a high transition temperature compared with the conventional phonon-driven superconductors. This high transition temperature suggests that the superconductivity is caused by the same interactions that lead to the Mott insulator which in turn could explain the unusual energy scales involved.

The various copper oxide superconductors share one common feature which are the 2 dimensional copper-oxygen planes. In these planes the copper atoms form a regular square lattice. Every two neighboring copper atoms share an oxygen atom. The rest of the material serves as a charge reservoir and separates the copper-oxygen layers. The first task is therefore to understand the physics of the CuO_2 planes. For a two dimensional system there cannot be superconducting long-range order but only a power law decay at finite temperature as shown by Hohenberg[1]. However, there can be a Kosterlitz-Thouless transition[2] at finite temperature and the system shows zero resistance even above zero temperature[3]. Similarly, there can be no antiferromagnetic long-range order[4] at finite temperature. In both cases a small 3-dimensional coupling can stabilize the groundstate of the 2-dimensional planes even at finite temperature. To understand the cuprates it is then important to investigate the nature of the groundstate and the lowest excited states of the CuO_2 planes.

The proximity to a Mott insulator also means that the correlations between the electrons will not be screened. The models will therefore describe strongly correlated electrons for which mean field descriptions do not provide a good starting point for perturbation expansions. To date, the most powerful methods for dealing with strongly correlated electron systems are to a large extent numerical. It is also the

aim of this work to provide additional numerical evidence for the presence or absence of superconductivity in the groundstate of strongly correlated models.

The models which are introduced in the following sections are among the simplest to describe strongly correlated electron systems. There has been a lot of research devoted to these models. The discovery of high T_c superconductors has been a stimulus to this interest so that a vast literature exists on the subject. A review over the current understanding can be found in the reviews by Dagotto[5], Kampf[6], and Brenig[7]. A compact exposition of the problem of strongly correlated electrons in general and the high T_c superconductors in particular can be found in Fulde's book[8].

1.1 The Three-Band Hubbard Model

As a first step towards a description of the CuO_2 planes we identify the relevant orbitals of the copper and oxygen atoms. These are the 3d orbitals for the Cu and the 2p orbitals for the oxygens. All other orbitals are either well below or well above the Fermi energy. Neglecting hybridization and the interactions between the electrons, the oxygen p-orbitals would be filled, whereas the copper d-orbitals have 1 hole per site, for the insulating compounds. Due to the lattice structure the orbital with $d_{x^2-y^2}$ character will contain this hole. Since this is closer to the configuration $\text{O-}2p^6 \text{ Cu-}3d^{10}$ where these orbitals are all filled, it is convenient to use this as the vacuum and work in the hole representation. Between the $d_{x^2-y^2}$ -orbital and the p-orbitals which point towards the Cu atoms there is a strong hybridization, which is described by the hopping term with coefficient t_{pd} in Eq. 1.1. Furthermore, the coulomb repulsion of two holes on the same Cu (U_d -term) or O site (U_p -term) as well as on neighboring Cu and O sites (U_{pd} -term) has to be taken into account. Together with the on-site energies ϵ_d and ϵ_p and an oxygen-oxygen hopping t_{pp} we then arrive at the Hamiltonian

$$\begin{aligned}
\mathcal{H} = & - t_{pd} \sum_{i,\tau,\sigma} \left(p_{i,\sigma}^\dagger d_{i+\tau,\sigma} + \text{h.c.} \right) - t_{pp} \sum_{i,\tau \neq \tau',\sigma} \left(p_{i+\tau,\sigma}^\dagger p_{i+\tau',\sigma} + \text{h.c.} \right) \\
& + \epsilon_d \sum_i n_i^d + \epsilon_p \sum_i \left(n_{i+\hat{x}/2}^p + n_{i+\hat{y}/2}^p \right) \\
& + U_p \sum_i \left(n_{i+\hat{x}/2\uparrow}^p n_{i+\hat{x}/2\downarrow}^p + n_{i+\hat{y}/2\uparrow}^p n_{i+\hat{y}/2\downarrow}^p \right) \\
& + U_d \sum_i n_{i\uparrow}^d n_{i\downarrow}^d + U_{pd} \sum_{i,\tau} n_i^d n_{i+\tau}^p
\end{aligned} \tag{1.1}$$

where the i run over the Cu sites and $\tau \in \{\pm\hat{x}/2, \pm\hat{y}/2\}$ points to the O sites. $p_{i+\tau}^\dagger$ and d_i^\dagger are the fermionic creation operators for the oxygen p- and copper d-orbitals. The parameters have been estimated by a constrained density functional method by

Hybertsen *et al.*[9] to be (in eV)

$\epsilon_p - \epsilon_d$	t_{pd}	t_{pp}	U_d	U_p	U_{pd}
3.6	1.3	0.65	10.5	4	1.2

These values are in agreement with electron energy loss spectroscopy (EELS) experiments by Nücker *et al.*[10]. Already for the terms included in the 3-band Hubbard model one can see that $U_{pd} < U_d, U_p$ and $t_{pp} < t_{pd}$. It is then reasonable to neglect contributions for the larger distances.

1.2 The t - J Model

The 3-band Hubbard model presented in the previous section is still too complicated to be treated either numerically or analytically. Its low energy physics can be captured with the t - J model as shown by Zhang and Rice[11]. The oxygen p-orbitals surrounding each Cu site can be replaced by linear combinations with $d_{x^2-y^2}$ - and s-like symmetry. Due to their symmetry, the s-like orbitals will not hybridize with the copper $d_{x^2-y^2}$ and form an band which is completely filled. The other band will hybridize via t_{pd} with the Cu d-orbital and an additional hole will form a singlet with the hole on the Cu site (Zhang-Rice singlet). The strong Coulomb repulsion effectively suppresses double occupancy, so that the kinetic energy is given by the Gutzwiller projected hopping. Furthermore, due to the overlap on the oxygens, antiparallel spins on neighboring Cu have a lower energy, yielding a antiferromagnetic exchange coupling. This leads to the t - J model

$$\mathcal{H} = -t \sum_{\langle i,j \rangle, \sigma} \left((1 - n_{i,-\sigma}) c_{i\sigma}^\dagger c_{j\sigma} (1 - n_{j,-\sigma}) + \text{h.c.} \right) + J \sum_{\langle i,j \rangle} \left(\mathbf{S}_i \cdot \mathbf{S}_j - \frac{1}{4} n_i n_j \right) \quad (1.2)$$

where the $c_{i\sigma}^\dagger$ are the creation operators for the new orbitals. By comparing the low energy spectrum of the 3-band Hubbard model and the t - J model for small clusters Hybertsen *et al.*[12] have found the parameters for the t - J model as $t=0.43\text{eV}$ and $J=0.128\text{eV}$. Of these two values the antiferromagnetic coupling J agrees very well with experiments, whereas t is less accurately known. Furthermore, it is likely that the kinetic energy is modified slightly with a next nearest neighbor hopping term with $t' < 0$.

1.3 The One-Band Hubbard Model

Another model which has been receiving a lot of attention is the original (1-band) Hubbard model[13, 14].

$$\mathcal{H} = -t \sum_{\langle i,j \rangle, \sigma} \left(c_{i\sigma}^\dagger c_{j\sigma} + \text{h.c.} \right) + U \sum_i n_{i\uparrow} n_{i\downarrow} \quad (1.3)$$

This corresponds to a description of the CuO₂ planes starting from the 3-band Hubbard model when $\epsilon_p - \epsilon_d > U_d \gg t_{pd}$. Hybertsen *et al.*[12] also compared the low-energy spectrum of the 1-band Hubbard model to the 3-band Hubbard model and arrived at the values $t=0.43\text{eV}$ and $U=5.4\text{eV}$, *i.e.*, $U/t \sim 12$, which is a bit more than the bandwidth.

It should be noted that the $1/U$ expansion of the 1-band Hubbard model also leads to the t - J model, with $J = \frac{4t^2}{U}$. Such an expansion also generates a 3-site term of the form

$$\mathcal{H}_3 = -J' \sum_{i,\tau \neq \tau',\sigma} \left(\tilde{c}_{i+\tau,\sigma}^\dagger \tilde{c}_{i,-\sigma}^\dagger \tilde{c}_{i,-\sigma} \tilde{c}_{i+\tau',\sigma} + \tilde{c}_{i+\tau,-\sigma}^\dagger \tilde{c}_{i,\sigma}^\dagger \tilde{c}_{i,-\sigma} \tilde{c}_{i+\tau',\sigma} \right) \quad (1.4)$$

with $\tilde{c}_{i\sigma}^\dagger = (1 - n_{i,-\sigma})c_{i\sigma}^\dagger$ for constraint hopping to prevent double occupancy. In the expansion $J' = \frac{t^2}{U}$ is of comparable magnitude as J . Of course, such a 3-site term also appears in a direct derivation of the t - J model from the 3-band Hubbard model. However, it will in general not have a coefficient which is fixed relative to the J -term. Due to the overlap of the hybridized orbitals on the oxygen sites J will be considerably larger than J' . Some of the differences between the strong coupling 1-band Hubbard model and the t - J model may be attributed to this 3-site term.

1.4 Some Known Results about the t - J Model

In the following we will describe some of the known results and open questions about the t - J model. Again, for a more complete overview one should consult the recent reviews on the subject[5, 6, 7].

1.4.1 Magnetic Order

For half-filling (*i.e.*, one electron per Cu site in the Zhang-Rice orbital) the t - J model reduces to the Heisenberg model. The electrons cannot move due to the constraint of no double occupancy and only the spin exchange interaction is relevant. It is generally agreed that the antiferromagnetic Heisenberg model provides an accurate description of the undoped parent materials[15].

Experimentally antiferromagnetic long-range order is characterized by a finite ordering Néel temperature T_N . For the undoped materials T_N is typically 300 K. This long-range order is also observed in doped materials with low hole doping. However, T_N is quickly suppressed with hole doping and for more than about 0.02 holes per copper site (in La₂CuO₄) the long-range order is completely suppressed(see, *e.g.*, Birgeneau[16], or Keimer *et al.*[17]). Compounds with larger doping only show short-range antiferromagnetic order characterized by a finite correlation length which is roughly the average separation distance between the holes[18].

The short-range order persists up to high dopings and even into the superconducting region[18, 19, 20, 21, 22, 23, 24]. Furthermore, neutron scattering experiments have revealed incommensurate spin fluctuation for $\text{La}_{2-x}\text{Sr}_x\text{CuO}_4$ with $x = 0.075$ and $x = 0.14$ [24, 25], where the peak at (π, π) splits and moves towards $(\pi, 0), (0, \pi)$. However, no static incommensurate order has been observed (as in the three dimensional Mott-Hubbard system V_{2-y}O_3).

In the t - J model the movement of the holes destroys the antiferromagnetic alignment of the spins and leads to a suppression of the long-range order. This has been verified by variational Monte Carlo, which finds a rapid suppression of antiferromagnetism with doping[26, 27]. The magnetic properties of the t - J model have been investigated in more detail by Singh and Glenister[28] using high-temperature expansion. They find a sharp antiferromagnetic peak in the spin-spin structure factor at half filling compatible with antiferromagnetic long-range order. At finite doping this peak is still present although it is suppressed. Furthermore they find (short-range) incommensurate spin order at higher dopings. These results suggest that the t - J model is able to explain the main features of the magnetism in the cuprates.

Another type of magnetic order, ferromagnetism, occurs at low hole doping for small antiferromagnetic coupling $J \ll t$. For one hole Nagaoka's theorem[29] states that the groundstate is a fully polarized ferromagnet. This does not address a finite density in the thermodynamic limit directly, but high-temperature expansion[30] and exact diagonalizations of small cluster[31] find a ferrimagnetic (*i.e.*, not fully polarized) region at small hole doping for $J/t < 0.1$.

1.4.2 Hole Binding and Phase Separation

If $J \gg t$ then the energy in the t - J model is determined by the Heisenberg term alone and the system tries to align as many neighboring spins as possible antiparallel. When holes are present they break the adjacent bonds. To lower the energy the holes will cluster together so that they break the fewest number of bonds. The system will separate into a completely antiferromagnetically aligned and an empty phase[32]. This phase separation will persist even when the kinetic energy becomes more important. However, the empty phase will be replaced by a phase with a finite density of electrons.¹ The line of phase separation has been determined by high-temperature expansion in one[33] and two dimensions[34].

It is still an open question, which is the lowest J/t necessary for phase separation. While Emery *et al.*[32] conjectured that phase separation would occur at all values of J the high-temperature expansion by Putikka *et al.*[34] clearly shows a finite critical

¹In one dimension at intermediate values of J/t the phase separation occurs between a phase with finite density and the *empty* phase[33].

value for $J_{\text{PS}} \sim 1.2t$. Putikka *et al.* also note that the phase separation line in 2D behaves rather different than in 1D where the phase separation line is at higher J for lower hole densities. They attributed this to the larger spin disturbance around the hole in 2D. This was also simulated in 1D by Prelovšek, Bonča, and Sega[35] by adding a longer-range spin exchange which lead to a behavior consistent with 2D. It is clear that in 2D (as opposed to 1D) the holes can arrange in a variety of ways. Recently, Prelovšek and Zotos[36] have investigated the arrangement of 2 and 4 holes on systems of 18, 20, and 26 sites using exact diagonalization and extrapolations from a restricted basis set. They find that from $J > J_c \sim 0.2t$ to $J < J_s \sim 1.5t$ the holes form independent pairs while above J_s they tend to align in the (1,0) or (0,1) direction before the compact clustering of phase separation begins to dominate at higher $J > J_s^* \sim 2.5t$. From their calculations one can conclude that a tendency towards a “striped phase” with the holes forming domain walls corresponding to a charge density wave (CDW) and a spin density wave (SDW) is realized before charge separation sets in. Many calculations may therefore underestimate the phase separation line. The incommensurate SDW could also explain the splitting of the peak at (π, π) for the short-range AF order as discussed above.

1.4.3 Superconductivity

Many of the methods that were successful in establishing results on the spin order or phase separation have not been able to provide evidence for or against superconductivity. Due to the sign problem quantum Monte Carlo methods were not able to reach low enough temperatures to show clear signals of superconductivity (*e.g.*, see Imada and Hatsugai[37], Imada[38], and Moreo[39]). With high-temperature expansions the pair-pair correlation functions have not yet been investigated. It is also not clear, whether series of high enough order can be calculated to reach a temperature below which a signal of superconductivity would be observed.

Recently, there has been some progress in the search for superconductivity. In order to form a condensate, the system should contain enough holes. For a 4×4 system the case of quarter filling is the most likely candidate for a condensate. Indeed, Dagotto and Riera find a strongly enhanced pair-pair structure factor[40]. Their result indicates that the superconductivity is most likely of $d_{x^2-y^2}$ symmetry. However, one should notice that the 4×4 system is still quite small with a largest separation of two points of about $2\sqrt{2} \approx 2.8$ (using periodic boundary conditions). Much of the signal may therefore be due to short-range correlations. Nevertheless, it provides a strong indication for the existence of d-wave superconductivity in the t - J model. Results for bigger clusters of up to 26 sites have been obtained by Ohta *et al.*[41]. They investigated the anomalous Green’s function and were able to fit

their data to a BCS ansatz. The d-wave gap which they observe grows roughly linearly with J .

For the 1-band Hubbard model Monthoux and Scalapino[42] have used a conserving fluctuation exchange approximation to obtain a self-consistent solution for the momentum- and frequency-dependent gap. They find a symmetry for the gap of $d_{x^2-y^2}$ type. The low temperature magnitude for the gap is very large with $2\Delta(0)/kT_c \sim 10$. Because of their calculation is performed on a large lattice of 128×128 sites the finite size effects will be very small. However it is unclear how much the conserving fluctuation exchange approximation affects the results.

Even though direct evidence for superconductivity is limited, there are variational calculations which favor superconductivity. However, they can only provide indirect evidence, because their bias. The variational wavefunctions are chosen from a limited set and cannot rule out some other groundstate with a different order not contained in this set. This is especially true for the case of the t - J model where various magnetic phases and phase separation are competing and may be the dominant instability. Nevertheless, variational studies provide useful information about the relative stability of phases and are a good starting point for further investigations. For the Hubbard model Yokoyama and Shiba[43] found d-wave superconductivity to be most favorable. For the t - J model including the 3-site term, *i.e.*, the strong coupling limit of the 1-band Hubbard model, Chen *et al.*[44] and later more detailed Li *et al.*[45] also found the d-wave state to have the lowest energy from a critical hole density of a few percent onwards, where antiferromagnetic order is suppressed. For higher dopings above 10 % where the 3-site term becomes important they find a mixed s+id state to be energetically favorable. Giamarchi and Lhuillier[27] also investigated the t - J model (without the 3-site term) and found the d-wave state to be stable up to a hole density of about 0.4. Furthermore, attempts have been made to improve the variational state using the power method[46, 47, 48] but these calculations are currently restricted to rather low electron densities. However they are able to address the question of the presence of a Luttinger-Liquid, which has also been investigated by variational wavefunctions[49, 50].

Chapter 2

The Method

The work presented in this thesis relies heavily on the Rayleigh-Ritz variational principle. With the availability of computers this method has become an important tool. Typically the necessary expectation values are computed by means of Monte Carlo sampling. This is possible for boson[51] as well as for fermion[52] systems. We defer the discussion about how the sampling is actually done to Chapter 3 and concentrate here on the physically important aspects of the method.

2.1 The Rayleigh-Ritz Principle and Generalizations

The Rayleigh-Ritz variational principle is one of the most powerful nonperturbative methods in quantum mechanics[53]. Given a system with a Hamiltonian \mathcal{H} , we can take any state $|\Psi\rangle$ from the Hilbert space, and we get an upper bound to the groundstate energy, E_0 , by

$$\frac{\langle\Psi|\mathcal{H}|\Psi\rangle}{\langle\Psi|\Psi\rangle} \geq E_0 \quad (2.1)$$

This can be easily seen, if we expand $|\Psi\rangle$ in terms of eigenstates $|n\rangle$ with energies E_n

$$\frac{\langle\Psi|\mathcal{H}|\Psi\rangle}{\langle\Psi|\Psi\rangle} = \sum_n E_n \frac{|\langle n|\Psi\rangle|^2}{\langle\Psi|\Psi\rangle} = E_0 + \sum_n (E_n - E_0) \frac{|\langle n|\Psi\rangle|^2}{\langle\Psi|\Psi\rangle} \geq E_0 \quad (2.2)$$

If we have a set of states we can choose the “best” approximation to the groundstate as the one with the lowest expectation value for the energy. However, we should keep in mind that the only rigorous result is the upper bound to the groundstate *energy*. There is no criterion about how close any *other* property of the groundstate is realized in this approximation.

Let us consider the following example. The Hartree-Fock method tries to find the best Slater determinant to approximate the groundstate, *i.e.*, the best wave function of an effective one-particle description. This will lead to a mean field theory, where

each electron experiences all the other electron as an averaged field. Starting from the mean field solution, perturbation theory can be used to obtain reliable quantitative results. The success of this approach is based on the observation that a weakly correlated system is already well described by independent electrons in an effective potential, and that the remaining part of the Hamiltonian constitutes a small perturbation. The variational principle is then not the only argument for the quality of the approximation. It mainly serves as a starting point for the perturbation analysis and implies that the inclusion of correlations beyond the mean field approximation will lower the energy.

This approach fails for strongly correlated systems. The remaining part that is not included in the effective Hamiltonian is not small enough to allow for a perturbation expansion. For the t - J model an effective one-particle description is even impossible because of the constraint of no double occupancy; most of the Slater determinants are not part of the Hilbert space. One then has to project out the double occupancy, which already induces some correlations between the electrons. For numerical calculations the projection to fulfill the constraint does not pose any particular problem. However, there is little control over the effect the projection has on the different mean field wavefunctions. Furthermore, most numerical calculations have to be done for finite systems, which leads to finite size effects. Nevertheless, one can still compare the expectation values for the projected wavefunctions corresponding to various mean field approaches. This provides some indication about which instability (magnetic, superconducting, *etc.*) is dominant.

Even for these strongly correlated systems we have some additional information about the quality of a variational wavefunction. The variance, or its square root the standard deviation, of the Hamiltonian measures the width of the energy distribution of a wavefunction. It provides a criterion for how much a wavefunction deviates from an eigenfunction[54]. The standard deviation $\sigma_{\mathcal{H}}$ of the Hamiltonian \mathcal{H} for a wavefunction $|\Psi\rangle$ is defined as

$$\sigma_{\mathcal{H}}^2 = \langle (\mathcal{H} - \langle \mathcal{H} \rangle)^2 \rangle = \frac{\langle \Psi | \mathcal{H}^2 | \Psi \rangle}{\langle \Psi | \Psi \rangle} - \left(\frac{\langle \Psi | \mathcal{H} | \Psi \rangle}{\langle \Psi | \Psi \rangle} \right)^2 \quad (2.3)$$

A wavefunction which is close to the groundstate will have both a low variational energy and a small variance close to zero; a small variance alone can also be achieved by converging to an excited eigenstate.

To obtain a more quantitative picture, let us consider a variational wavefunction which is constructed as a linear combination of just two eigenstates. The two eigenstates shall be a typical excited state with energy E_1 and the groundstate with energy E_0 . The probabilities for these eigenstates are ρ_1 and $\rho_0 = (1 - \rho_1)$, respectively. Then, we have for the energy expectation value \bar{E} and the standard deviation

σ

$$\bar{E} - E_0 = \rho_1(E_1 - E_0) \quad (2.4)$$

$$\sigma = \sqrt{\rho_1 - \rho_1^2}(E_1 - E_0) \quad (2.5)$$

If we keep E_1 fixed and use ρ_1 to describe the convergence to the groundstate, we can see that \bar{E} converges linearly in ρ_1 whereas σ decreases only proportional to $\sqrt{\rho_1}$. If E_1 is not kept constant or if more eigenstates are included in the variational wavefunction, then almost any behavior for \bar{E} and σ can be constructed. However, we can clearly see that when both \bar{E} and σ are lowered, more weight must be in the lower energy eigenstates. The additional information contained in σ is the relevant energy scale where the wavefunction has a considerable weight; for a given pair of values \bar{E} and σ , there is an upper bound for the weight at any energy E in an interval dE of $\rho(E)dE \leq \frac{\sigma^2}{(E-\bar{E})^2 + \sigma^2}$.

2.2 Systematic Improvement by Lanczos Iteration

If we want more information about the groundstate, we need higher moments of the Hamiltonian. Whereas the standard deviation is a measure of the width of the probability distribution $\rho(E)$, it doesn't tell us on which side of the mean value \bar{E} it extends farther. This information is contained in the skewness

$$\text{Skew}(\mathcal{H}) = \left\langle \left(\frac{\mathcal{H} - \langle \mathcal{H} \rangle}{\sigma_{\mathcal{H}}} \right)^3 \right\rangle \quad (2.6)$$

which contains the third moment of the Hamiltonian. Higher moments will contain even more information about the extent of the distribution.

To calculate the improved upper bound to the groundstate energy we can use the Lanczos scheme[55]. If we apply the Hamiltonian n times to the wavefunction, we can use the Rayleigh-Ritz principle for the ansatz

$$|\nu_0, \nu_1, \dots, \nu_n\rangle = \sum_{i=0}^n \nu_i \mathcal{H}^i |\Psi\rangle \quad (2.7)$$

As can easily be seen, we need all the moments up to order $2n + 1$ for n Lanczos iterations. For this new wavefunction we can then evaluate any other expectation value. *E.g.*, if we also want to know the new variance, we have to include the next even order moment (*i.e.*, $\langle \mathcal{H}^{2n+2} \rangle$) in our calculation. The Lanczos method is most easily expressed in terms of normalized basis states as obtained by the three term recurrence relation[56]

$$\begin{aligned} \mathcal{H}|\Psi_0\rangle &= a_0|\Psi_0\rangle + b_1|\Psi_1\rangle \\ \mathcal{H}|\Psi_n\rangle &= a_n|\Psi_n\rangle + b_n|\Psi_{n-1}\rangle + b_{n+1}|\Psi_{n+1}\rangle, (n \geq 1) \end{aligned} \quad (2.8)$$

where starting from $|\Psi_0\rangle = |\Psi\rangle/\sqrt{\langle\Psi|\Psi\rangle}$ a new orthonormal set of basis states $|\Psi_n\rangle$ is constructed in which the Hamiltonian has tridiagonal form, as can easily be seen. For the n -th Lanczos iteration only the subspace spanned by $|\Psi_0\rangle, \dots, |\Psi_n\rangle$ is considered. We then need the values of a_0, \dots, a_n and b_1, \dots, b_n . Using the notation $H_n = \langle\Psi_0|\mathcal{H}^n|\Psi_0\rangle$ and $h_n = \langle\Psi_0|(\mathcal{H}-H_1)^n|\Psi_0\rangle = \sum_{i=0}^{n-2} (-1)^i \binom{n}{i} H_{n-1} H_1^i - (n-1)(-1)^n H_1^n$ we obtain for the first few coefficients

$$\begin{aligned}
a_0 &= H_1 \\
b_1 &= \sqrt{h_2} \\
a_1 &= H_1 + \frac{h_3}{h_2} \\
b_2 &= \frac{\sqrt{h_4 h_2 - h_3^2 - h_2^3}}{h_3} \\
a_2 &= H_1 + \frac{h_5 h_2^2 + h_3^3 - 2h_4 h_3 h_2}{h_2(h_4 h_2 - h_3^2 - h_2^3)}
\end{aligned} \tag{2.9}$$

A further reduction from tridiagonal to diagonal form is in general not possible in a finite number of steps, and one has to resort to iterative methods. The QR and QL algorithms are often used as they are numerically stable and fast converging[57, 58, 59]. A general presentation of available methods can be found in Ref. [60].

2.3 Limitations for Higher Moments and the Sign Problem

While the above description of the Lanczos method as a variational approach is mathematically straightforward, it has some inherent limitations. In the usual formulation of the Lanczos method a new state is generated and has to be stored. For each iteration the last two states are needed, so that the new state can replace the one but last state. Each iteration then takes about the same amount of computing time and the method is limited by the memory requirements to store the two states.

In the variational formulation of the Lanczos method of section 2.2 the new states are given implicitly by polynomials of the Hamiltonian applied to the initial trial wavefunction. This obviates the problem of memory consumption but the time required for the evaluation of the moments grows exponentially with the number of Lanczos steps. *I.e.*, if we use a complete set of basis states, *e.g.*, the configuration basis $|\mathbf{R}\rangle$ we have

$$\langle\mathcal{H}^n\rangle = \sum_{\mathbf{R}_1, \mathbf{R}_2} \langle\Psi_0|\mathbf{R}_1\rangle \langle\mathbf{R}_1|\mathcal{H}^n|\mathbf{R}_2\rangle \langle\mathbf{R}_2|\Psi_0\rangle \tag{2.10}$$

With higher order n the number of terms grows exponentially, which is the main

reason for the increased time requirements. Using Monte Carlo sampling we will only have to evaluate a fraction of all the terms, but the expectation values will be known only within a statistical error. It is then important to find out up to what accuracy the moments have to be known, and how small a fraction of the terms (*i.e.*, how little computing time) it takes to reach this accuracy. It turns out that in general the eigenvalues of the Hamiltonian in the subspace corresponding to a finite number of Lanczos iteration are more sensitive to deviations in the higher moments. However, not all eigenvalues suffer this sensitivity in the same way. It is interesting to discuss this issue in more detail.

This fact, that the error bars get bigger with the number of iteration, is sometimes referred to as another manifestation of the fermion sign problem of quantum Monte Carlo. Superficially, especially from a practical point of view, this may be a reasonable terminology. In both cases the quality of the initial trial wavefunction determines how fast the iterations converge to the groundstate, and whether the convergence is achieved before the errors make the result useless. However, there are important differences to the fermion sign problem, which may lead to different approaches for a solution. The big errors of the higher order iterations are not caused by the fermionic nature of problem. Finding the eigenvalues of an operator from the moments is one example of an *inverse problem*, which are often “ill-conditioned” [57]. Given any (Hermitian) operator, in our case the Hamiltonian \mathcal{H} , and a wavefunction in its spectral decomposition

$$\mathcal{H} = \sum_i E_i |i\rangle\langle i| \quad (2.11)$$

$$|\Psi\rangle = \sum_i \alpha_i |i\rangle \quad (2.12)$$

we can write the moments as

$$H_n = \langle \Psi | \mathcal{H}^n | \Psi \rangle = \sum_i |\alpha_i|^2 E_i^n = \sum_i \rho_i E_i^n \quad (2.13)$$

i.e., the moments H_n are a function of the weights $\rho_i = |\alpha_i|^2$ and eigenvalues E_i . This is numerically very stable, whereas the *inverse problem* of finding the energies E_i and weights ρ_i from the moments H_n is very sensitive to small deviations, *e.g.*, rounding or statistical errors.

Obviously, the uncertainty in the E_i depends on the initial wavefunction $|\Psi\rangle$. Furthermore, not all of the E_i will suffer from deviations in the moments in the same way. As a limiting case, let us consider the wavefunction $|\Psi\rangle = |0\rangle$, *i.e.*, $\rho_0 = 1, \rho_i = 0 (i \geq 1)$. Then $E_0 = H_1$ is already known from the first moment without loss of accuracy and the higher moments contain no additional information. For a small perturbation in the ρ_i , the higher moments start to contain the information about the

corresponding E_i , but will be very sensitive to small deviations. One of the excited E_i might enter then with such a large error, that it will be mistaken for the smallest eigenvalue. For the Monte Carlo sampling the error can be measured, so that this situation is easily revealed. However, a naive application of the Lanczos method, which just calculates the lowest eigenvalue, becomes unstable when increasing the number of iterations. Paradoxically, starting with a “better” wavefunction (*i.e.*, with smaller $\rho_i, i \geq 1$) amplifies this instability.

The information of E_0 is obviously still contained in the moments H_n , and we need a way to extract it. For n Lanczos iterations we obtain an $n + 1$ dimensional subspace, and correspondingly an $(n + 1) \times (n + 1)$ tridiagonal matrix for the Hamiltonian. If we determine all eigenvalues of this matrix, we can separate those with large from those with small errors. This allows us to calculate some eigenvalues with a reasonable accuracy, without the need of excessive Monte Carlo sampling of the higher moments. Alternatively we can variationally find a state in this $n + 1$ dimensional subspace, which minimizes both, the energy and its error according to some criterion.¹ This later approach will yield the best value possible that matches the criterion.

A somewhat simpler approach to increase the stability is to use the power method. The sequence of wavefunctions $|\phi_n\rangle = (\mathcal{H} - W)^n|\Psi\rangle$ increases the weight of the eigenfunction with the largest absolute value of $E_i - W$. For an appropriate W this will be the groundstate energy E_0 . $|\phi_n\rangle$ converges to the groundstate for $n \rightarrow \infty$. $\langle \mathcal{H}^{2n+1} \rangle / \langle \mathcal{H}^{2n} \rangle$ converges to E_0 from above. As can easily be seen, this value cannot provide a better variational upper bound as the approach described in the last paragraph. However, it is considerably easier to calculate, and may be the optimal method to analyze the higher moments. For the t - J model Chen and Lee[61, 46, 47] have successfully used this method with up to 20 iterations.

A related issue concerns the case when two energies are much closer than the typical energy differences, *e.g.*, $|E_i - E_j| \ll \sigma_{\mathcal{H}}$. Then they contribute to the moments almost as if it was one degenerate energy level. To resolve the individual energy levels requires then in general many iterations and moments known with a high accuracy. For any realistic calculation it is therefore virtually impossible to resolve energy levels, which are much closer than one standard deviation.

From the discussion in this section we can conclude that the requirements for the initial trial wavefunction are:

(a) there must be a substantial weight for the eigenfunctions whose energy we want to determine; *i.e.*, $\rho_0 \gg \rho_i$ except for n values of i , if we want to determine the groundstate energy E_0 in n iterations.

¹*E.g.*, we can minimize the energy plus one standard deviation.

(b) $\sigma_{\mathcal{H}} = \langle \mathcal{H}^2 \rangle - \langle \mathcal{H} \rangle^2$ should be small, *e.g.*, on the order of the energy level spacing we want to resolve. Alternatively, $\sigma_{\mathcal{H}}$ defines the energy scale which can easily be resolved and energy levels which are much closer to each other require a high accuracy, *i.e.*, long computing times to be distinguished.

2.4 Separate Treatment of the Short- and Long-Range Behavior

As we have seen in the previous sections, a straightforward combination of the Lanczos method and the variational Monte Carlo approach leads to large errors even for a moderate number of iterations or, equivalently, requires excessive computing time to achieve a reasonable accuracy. Practical applications of this method are then restricted to one or at most two iterations. Under these conditions it is essential to make optimal use of this one iteration and to extract as much information as possible.

Let us consider the effect of one Lanczos iteration. Many typical Hamiltonians in solid state physics are short-ranged. The t - J model is an example where the terms are restricted to nearest neighbors, and even in more generalized versions the contributions become negligible when they extend over a few lattice spacings only. An ordered phase like superconducting order is on the other hand characterized by a certain long-range behavior. Starting from a general wavefunction without any specific properties (like a random wavefunction in a typical Lanczos application for exact diagonalization) n Lanczos iteration will change the correlations in the wavefunction only on a length scale of na if a is the characteristic length scale of the Hamiltonian (*i.e.*, $a =$ one lattice spacing in the t - J model). If we want to investigate the presence or absence of an ordered phase, where the long-range order is established at a characteristic length ξ , we would at least need ξ/a iterations to obtain reliable results[56].

The standard Rayleigh-Ritz variational Monte Carlo approach typically uses wavefunctions from a mean-field ansatz. These wavefunctions have a certain long-range behavior built in, which is controlled by a variational parameter. The long-range order is then well-described, but there is no control over the short-range part of the wavefunction. For a system like the t - J Hamiltonian with strong short-range correlations we cannot know how well the optimal variational wavefunction reflects the long-range behavior of the groundstate, or whether it tries to achieve a compromise to gain energy with the strong local terms of Hamiltonian.

The combined method can make use of the advantages of both methods. If we start with a variational wavefunction which describes the right long-range behavior

for the groundstate, then the Lanczos steps only have to adjust the short-range part and only a few iterations are necessary to obtain a reliable approximation for the groundstate. We can generalize the Lanczos steps not to use the Hamiltonian but the most general linear combination of operators, which act on the same length scale as the Hamiltonian and preserve its symmetries. Such operators can be constructed systematically as is shown in section 2.6; *e.g.*, if we restrict the operators to act on nearest neighbor sites we end up with the same terms as in the t - J - V model, but with arbitrary coefficients independent of the coefficients in the Hamiltonian. With these generalized Lanczos operators already one iteration will yield an approximation of the groundstate which incorporates the relevant features.

The remaining problem is then to find a criterion for when a wavefunction has the right long-range behavior to be a good starting point for the iteration. The energy does not provide this criterion, since from the energy alone the long-range order may be over- or underestimated due to the short-range nature of the Hamiltonian. However, we can use an indirect approach. If we start with a long-range order which is too large, the Lanczos iterations will gradually shift the weight towards smaller distances in order to suppress the long-range order. If on the other hand we start with too small a long-range order, it will analogously be enhanced. The right long-range behavior will be characterized by the fact that it is left unchanged by the Lanczos iteration. This method can be thought of as “measuring” the long-range behavior of the groundstate, by adjusting the long-range order until a local perturbation will not affect it anymore.

2.5 Non-Variational Results from One Lanczos Iteration

There is another way to extract more information from one (generalized) Lanczos iteration. If we consider Eqns. (2.4) and (2.5) we can see that both $\bar{E} - E_0$ and σ^2 vanish linearly with ρ_1 for small values of ρ_1 . This should still be approximately true for the case of a wavefunction which has most of its weight in the groundstate at E_0 and the small remaining contributions are dominated by an energy E_1 . We can then use the two values of \bar{E} and σ^2 before and after the iteration to extrapolate to $\sigma^2 = 0$ and obtain an estimate for E_0 . This estimate will not be a variational bound and it will also only be meaningful for a good starting wavefunction. *I.e.*, only after we have confirmed by the other criteria mentioned above that a wavefunction is a good starting point for the iteration, we can use the extrapolation to obtain an improved estimate for the groundstate energy. Furthermore, the extrapolation from a set of wavefunctions close to the optimal may provide some indication of the error we can

expect for the extrapolated energy.

2.6 Generalized Lanczos Operators

In section 2.4 we mentioned the use of generalized Lanczos operator to achieve the optimal improvement in one iteration. These operators can be constructed systematically.

E.g., the most general operator, which acts on nearest neighbors only, is a linear combination of $c_{i,\sigma_1}^\dagger c_{j,\sigma_2}$, $c_{i,\sigma_1}^\dagger c_{j,\sigma_2}^\dagger c_{j,\sigma_3} c_{i,\sigma_4}$, and $c_{i,\sigma_1}^\dagger c_{i,\sigma_2}^\dagger c_{j,\sigma_3} c_{j,\sigma_4}$, where $\langle i, j \rangle$ runs over all nearest neighbor pairs and $\sigma_1, \dots, \sigma_4$ take on any combination of the spin projections (up or down, each). With the constraint of no double occupancy we can leave out the last of the three sets. For other clusters than a nearest neighbor pair there are analogous sets of operators.

Most of the linear combinations obtained in this way don't preserve the symmetry of the wavefunction. *E.g.*, starting from a translationally invariant wavefunction they will mix in states with momenta different from $\mathbf{k} = 0$, and analogously they will mix different spin excitations. If we want to investigate wavefunctions belonging to a specific symmetry, we want to restrict the operators to those that leave the symmetry invariant. This can be done by group theoretical projections onto invariant representations[62, 63]. The space group symmetry is easily taken into account. The whole cluster has to be translated and rotated in all possible ways and the obtained operators have to be added.

The spin symmetry is a bit more involved. We have to perform the projection for the continuous rotation group. Using the Euler angle representation, we obtain the symmetric part \mathcal{A}_S of an operator \mathcal{A} with

$$\mathcal{A}_S = \frac{1}{8\pi^2} \int_0^{2\pi} d\alpha \int_{-1}^1 d(\cos\beta) \int_0^{2\pi} d\gamma U(\alpha, \beta, \gamma) \mathcal{A} U(\alpha, \beta, \gamma)^{-1} \quad (2.14)$$

The creation- and annihilation-operators transform as

$$U c_\sigma^\dagger U^{-1} = e^{-i\sigma\alpha/2} \cos(\beta/2) e^{-i\sigma\gamma/2} c_\sigma^\dagger + \sigma e^{i\sigma\alpha/2} \sin(\beta/2) e^{-i\sigma\gamma/2} c_{-\sigma}^\dagger \quad (2.15)$$

$$U c_\sigma U^{-1} = e^{i\sigma\alpha/2} \cos(\beta/2) e^{i\sigma\gamma/2} c_\sigma + \sigma e^{-i\sigma\alpha/2} \sin(\beta/2) e^{i\sigma\gamma/2} c_{-\sigma} \quad (2.16)$$

In the projection of a product of several creation- and annihilation-operators the integrals over α and γ select the possible combinations of spin projections and define the relative signs between them, while the integral over β leads to the non-trivial coefficients of the form

$$\int_{-1}^1 d(\cos\beta) \cos^{2(n-m)}(\beta/2) \sin^{2m}(\beta/2) = \frac{2}{(n+1) \binom{n}{m}} \quad (2.17)$$

These operations can be incorporated in a program without any problems, so that we are able to generate a suitable set of linearly independent operators, which preserve the symmetries of the Hamiltonian.

For small clusters there are only a few operators, so that we are left with a manageable set of variational parameter for the Lanczos iteration. For the case of the nearest neighbor operators we obtain the familiar three operators

$$\mathcal{A}_1 = \sum_{\langle i,j \rangle, \sigma} \left(\tilde{c}_{i,\sigma}^\dagger \tilde{c}_{j,\sigma} + \tilde{c}_{j,\sigma}^\dagger \tilde{c}_{i,\sigma} \right) \quad (2.18)$$

$$\mathcal{A}_2 = \sum_{\langle i,j \rangle} \mathbf{S}_i \mathbf{S}_j \quad (2.19)$$

$$\mathcal{A}_3 = \sum_{\langle i,j \rangle} n_i n_j \quad (2.20)$$

Of course, these operators are only defined up to linear combinations of each other, and to obtain the most general operator we have to add them with arbitrary coefficients, *i.e.*, $\alpha_0 + \alpha_1 \mathcal{A}_1 + \alpha_2 \mathcal{A}_2 + \alpha_3 \mathcal{A}_3$. The most important of these operators will generally have a close connection to the Hamiltonian[64]

2.7 Wavefunctions

One main restriction in a variational approach is given by the types of wavefunctions that are considered. This determines how close in energy we can approximate the groundstate before the Lanczos iteration. However, we have found in section 2.4 that the energy alone is not a good criterion for the properties of the groundstate. We then prefer to use wavefunctions with a slightly less optimal energy but with a well defined long-range behavior. The generalized Lanczos iteration will then take care of most of the remaining correlations. The main task is then to use wavefunctions which can be evaluated efficiently. Two of the most commonly used types of wavefunctions are the Slater determinants and the resonant valence bond (RVB) wavefunction[65]. Neither the Slater determinant nor the RVB wavefunction will in general obey the constraint of no double occupancy. We can enforce this with a projection as follows

$$|\Psi\rangle = \mathcal{P}_G |\Psi_0\rangle = \prod_i (1 - n_{i,\uparrow} n_{i,\downarrow}) |\Psi_0\rangle \quad (2.21)$$

where $|\Psi_0\rangle$ is the original Slater determinant or RVB wavefunction. $|\Psi\rangle$ will then already contain some correlations, *i.e.*, it will no more be a Slater determinant or RVB wavefunction, respectively. Furthermore $|\Psi\rangle$ will in general not be normalized when $|\Psi_0\rangle$ was. The projection will be taken care of by using an appropriate set of basis states and we will also calculate $\langle \Psi | \Psi \rangle$ explicitly to obtain properly normalized

results. Therefore, we only have to deal with $|\Psi_0\rangle$ and we have to specify it only up to an overall factor.

A Slater determinant is given by a set of one-particle orbitals $\varphi_l(\mathbf{R}_i, \sigma)$, or by the corresponding creation operators $c_l^\dagger = \sum_{i,\sigma} \varphi_l(\mathbf{R}_i, \sigma) c_{i,\sigma}^\dagger$. We obtain the wavefunction

$$|\Psi_0\rangle = \prod_l c_l^\dagger |0\rangle \quad (2.22)$$

$$\langle (\mathbf{R}_1, \sigma_1), \dots, (\mathbf{R}_N, \sigma_N) | \Psi_0 \rangle = \det \begin{pmatrix} \varphi_1(\mathbf{R}_1, \sigma_1) & \cdots & \varphi_1(\mathbf{R}_N, \sigma_N) \\ \vdots & \ddots & \vdots \\ \varphi_N(\mathbf{R}_1, \sigma_1) & \cdots & \varphi_N(\mathbf{R}_N, \sigma_N) \end{pmatrix} \quad (2.23)$$

Also the RVB wavefunctions can be written as determinants. They are characterized by a function $a(\mathbf{R}_\uparrow, \mathbf{R}_\downarrow)$ which specifies the strength of the valence bond between \mathbf{R}_\uparrow and \mathbf{R}_\downarrow .

$$|\Psi_0\rangle = \left(\sum_{\mathbf{R}_\uparrow, \mathbf{R}_\downarrow} a(\mathbf{R}_\uparrow, \mathbf{R}_\downarrow) c_{\mathbf{R}_\uparrow, \uparrow}^\dagger c_{\mathbf{R}_\downarrow, \downarrow}^\dagger \right)^{N/2} \quad (2.24)$$

$$\langle \mathbf{R}_{1,\uparrow}, \dots, \mathbf{R}_{N/2,\downarrow} | \Psi_0 \rangle = \det \begin{pmatrix} a(\mathbf{R}_{1,\uparrow}, \mathbf{R}_{1,\downarrow}) & \cdots & a(\mathbf{R}_{1,\uparrow}, \mathbf{R}_{N/2,\downarrow}) \\ \vdots & \ddots & \vdots \\ a(\mathbf{R}_{N/2,\uparrow}, \mathbf{R}_{1,\downarrow}) & \cdots & a(\mathbf{R}_{N/2,\uparrow}, \mathbf{R}_{N/2,\downarrow}) \end{pmatrix} \quad (2.25)$$

2.8 Lattices and Finite Size Effects

For all of the numerical calculation we have to choose a finite lattice. In order to reduce boundary effects, the finite lattice is repeated periodically in all spatial directions. These periods are described by a set of vectors with coordinates, which are integer multiples of the lattice constant. Although these vectors can be chosen quite general, we perform our calculation with sets, which are compatible with the lattice symmetry. For the case of the 2 dimensional square lattice considered in this work the available lattices are defined by the periods (n, m) and $(-m, n)$. Furthermore, if we want to investigate a bi-partite lattice there is an additional constraint that $n + m = \text{even}$.

Fig. 2.1 shows an example of a tilted lattice. It corresponds to the choice of $(n, m) = (7, 1)$, which is the lattice that is mostly used in this work. The deviations from the thermodynamic limit in the results are mainly determined by the number of points on the lattice. With the choice of a bigger lattice, such finite size effects can be reduced. However, the size of the Hilbert space and therefore the time requirements for the computation grows exponentially with the number of lattice sites. This sets an upper bound to the number of sites.

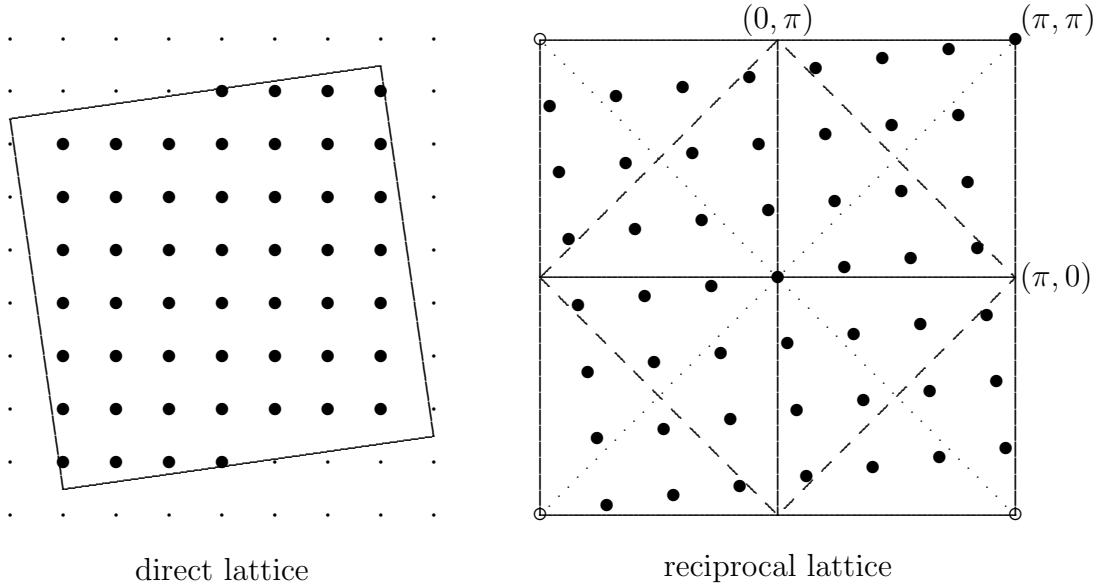


Figure 2.1: Example for a finite lattice with general boundaries. To model the infinite lattice, the finite lattice is repeated with periods (n, m) and $(-m, n)$. The number of sites in the finite lattice is $n^2 + m^2$. Also shown is the reciprocal lattice with the discrete set of \mathbf{k} -points corresponding to the finite lattice with periodic boundary conditions. For these figures we have chosen $(n, m) = (7, 1)$. The dashed line shows the Fermi surface for a tight binding model at half-filling, while the dotted line indicates the nodes corresponding to the symmetry $d_{x^2-y^2}$. For the lattice shown here non of the \mathbf{k} points lies on the Fermi surface and only $\mathbf{k} = 0$ and $\mathbf{k} = (\pi, \pi)$ are on the nodes. This will lead to smaller finite-size effects in the calculations reported in this work.

Additional finite size effects are caused by artificial degeneracies. The Fermi sea for a finite lattice is defined by occupying the N_e orbitals with the lowest $\epsilon(\mathbf{k})$. $\epsilon(\mathbf{k})$ is the dispersion given by the kinetic energy and N_e is the number of electrons. Due to the lattice symmetry there will in general be 4 \mathbf{k} -points with the same energy $\epsilon(\mathbf{k})$ which can each be occupied by an up- and a down-spin. Depending on the number of electrons there may be an arbitrary choice which of the \mathbf{k} orbitals to occupy. *E.g.*, if we assume the tight binding form $\epsilon(\mathbf{k}) = -\frac{W}{4}(\cos(k_x) + \cos(k_y))$ then the first electron will go into the $\mathbf{k} = 0$ -orbital. Due to its spin there is a 2-fold degeneracy of this state. The next electron will occupy the opposite spin projection in the same orbital, which yields a non-degenerate state. Filling in the next 7 electrons again leads to degenerate states as they can be distributed among the 4 next lowest \mathbf{k} -orbitals with the next lowest energy. Only the 10th electron fills this shell completely and leads again to a non-degenerate state. Whenever there are $8l + 2$ electrons (with l an integer) the $l + 1$ lowest shells will be closed and the Fermi sea is well defined, while any of the other (open shell) configuration is degenerate. In general, some variational wavefunctions will suffer from this problem and others will not. While it is technically not difficult to construct well defined wavefunctions even for the open shells (*e.g.*, by choosing an appropriately symmetrized linear combination), the degeneracy might lead to an artificially high energy and a correlated wavefunction may lower the energy mainly by removing this degeneracy. This is strictly a finite size effect, since in the thermodynamic limit there is no such degeneracy for any filling. When dealing with results on finite lattices we should expect to see variations with the number of electrons which are connected with these shell effects. If enough fillings are available for parameters which lead to the same groundstate, then a pattern with a period of 8 electrons will be superimposed on the results as a function of the number of electrons. Such a pattern can often help to estimate the magnitude of the finite size effects.

For the 50 sites lattice shown in Fig. 2.1 the half-filled case of one electron per site corresponds to a filled shell. The dashed line indicates the Fermi energy for the half-filled case using the tight binding form of $\epsilon(\mathbf{k})$ given above. The \mathbf{k} -points inside the dashed line correspond to filled orbitals of the Fermi sea.

An additional consideration for the choice of the lattice concerns the symmetry of the wavefunction. *E.g.*, in Fig. 2.1 the dotted line separates different sector corresponding to the relative sign of the $d_{x^2-y^2}$ symmetry. In the definition of the wavefunctions, nodes and poles will appear mainly at such special symmetry lines. *E.g.*, this will be the case for the Fourier transform of the bond strengths $\tilde{a}(\mathbf{k}) = \sum_{\mathbf{k}} \exp(i\mathbf{k}\Delta\mathbf{R})a(\Delta\mathbf{R})$ in the RVB pairing.

In order to avoid these symmetry related lines we can choose lattices with periods

$(n, 1)$ and $(-1, n)$ with n an integer, of which the 50 sites lattice is a special case. Such lattices tend to reduce the finite size effects.

Ideally, one would want to perform a finite size scaling using different lattice sizes. However this is only possible for certain fillings, since not all fillings are available for all lattice sizes. This restriction is even worse, if we want to compare closed shell configurations. In general we have to resort to qualitative estimates for when the finite size effects become negligible.

Chapter 3

Implementation of the Algorithm

In this chapter we would like to present some of the necessary details to obtain the results of this thesis. Although this information does not contribute to the understanding of the physics involved, it is essential when one is to estimate the validity of the results or their possible improvements.

3.1 Monte Carlo Sampling

For the strongly correlated fermion systems, which we are investigating, there are no analytic formulas available for the variational expectation values, except for some special cases like the Néel state. In general, we have to use a complete set of states and perform the sum over these states explicitly. Due to the constraint of no double occupancy of any one site, the most simple complete set of states is the configuration basis. Each member of this basis set is determined by the positions of all the up- and down-spin electrons. If we want to evaluate the expectation value of the Hamiltonian \mathcal{H} for a given wavefunction $|\Psi\rangle$ we obtain (where \mathbf{R} labels the configurations)

$$\langle\Psi|\mathcal{H}|\Psi\rangle = \sum_{\mathbf{R},\mathbf{R}'} \langle\Psi|\mathbf{R}\rangle\langle\mathbf{R}|\mathcal{H}|\mathbf{R}'\rangle\langle\mathbf{R}'|\Psi\rangle \quad (3.1)$$

If the wavefunction is not normalized we also have to evaluate $\langle\Psi|\Psi\rangle$ to obtain the energy. The number of terms $\langle\mathbf{R}|\Psi\rangle$ that appear in this sum is equal to the dimension of the Hilbert space. Even for moderate system sizes it becomes impractical to perform this calculation. However, we can estimate the sum by taking a subset of the terms at random (*i.e.*, “Monte Carlo sampling”). This subset serves as a representative sample which lets us extrapolate to the whole sum. This approach will succeed, if the individual terms in the sum show only little variation among each other. For a variational wavefunction $|\Psi\rangle$, which is close to the groundstate, we know $\mathcal{H}|\Psi\rangle \approx E_0|\Psi\rangle$. The ratio $\langle\mathbf{R}|\mathcal{H}|\Psi\rangle/\langle\mathbf{R}|\Psi\rangle$ shows only little dependence on \mathbf{R} and is well suited for a Monte Carlo evaluation.

In general, we want to evaluate a sum

$$F = \sum_x f(x)P(x) \quad (3.2)$$

where $P(x)$ is a probability distribution, *i.e.*, any function of x with $P(x) \geq 0$ and $\sum_x P(x) = 1$. We generate a sample X of values x drawn with the probability $P(x)$. This leads to an estimate for the value F

$$F \approx \tilde{F} = \frac{1}{N_X} \sum_{x \in X} f(x) \quad (3.3)$$

where N_X is the number of elements in the sample X . The Central Limit Theorem ensures that for big enough samples the values \tilde{F} are normal-distributed and converge within statistical error towards F . We obtain the statistical error by combining the estimates from independent samples X_i . The fact that the \tilde{F} follow a normal distribution allows one to perform various statistical tests[66]. Such tests are an invaluable tool during program development to uncover errors.

3.2 Importance Sampling

The choice of $P(x)$ in Eq. (3.2) is largely arbitrary. Any factorization will produce the same F and the only restriction is that $P(x)$ cannot be zero where the product $f(x)P(x)$ should be finite. If we choose $P(x)$ such that $f(x)$ is almost constant, then the Monte Carlo sampling will converge rapidly. Finding an optimal choice for $P(x)$ is known as *importance sampling*.

For Eq. 3.1 there is a well-known good choice with $P(\mathbf{R}) = |\langle \mathbf{R} | \Psi \rangle|^2 / \langle \Psi | \Psi \rangle$. Here, $P(\mathbf{R})$ can become zero, but only when the whole term in the sum is zero. Those terms don't contribute to the sum and can be neglected. The expectation value for the energy is then

$$\begin{aligned} \frac{\langle \Psi | \mathcal{H} | \Psi \rangle}{\langle \Psi | \Psi \rangle} &= \sum_{\mathbf{R}} \frac{\langle \mathbf{R} | \mathcal{H} | \Psi \rangle}{\langle \mathbf{R} | \Psi \rangle} P(\mathbf{R}) \\ P(\mathbf{R}) &= \frac{|\langle \mathbf{R} | \Psi \rangle|^2}{\langle \Psi | \Psi \rangle} \end{aligned} \quad (3.4)$$

For the more general expectation values like $\langle \Psi | \mathcal{A}_i \mathcal{H} \mathcal{A}_j | \Psi \rangle$ we have to use a different probability distribution, *e.g.*, we can use

$$\begin{aligned} \langle \Psi | \mathcal{A}_i \mathcal{H} \mathcal{A}_j | \Psi \rangle &= \sum_{\mathbf{R}} \frac{\langle \Psi | \mathcal{A}_i | \mathbf{R} \rangle \langle \mathbf{R} | \mathcal{H} \mathcal{A}_j | \Psi \rangle}{P_i(\mathbf{R})} P_i(\mathbf{R}) \\ P_i(\mathbf{R}) &= C_{P_i} |\langle \mathbf{R} | \mathcal{A}_i | \Psi \rangle|^2 \end{aligned} \quad (3.5)$$

The constant C_{P_i} is determined by the normalization of P_i .

To generate samples drawn from a probability distribution $P(\mathbf{R})$ we use the *Metropolis algorithm*[67]. Starting from a configuration \mathbf{R} a new configuration \mathbf{R}' is accepted if $P(\mathbf{R}') > P(\mathbf{R})$. Otherwise it is only accepted with a probability equal to $P(\mathbf{R}')/P(\mathbf{R})$. For long enough sequences these \mathbf{R} are distributed according to $P(\mathbf{R})$. In this scheme only ratios of the probabilities need to be calculated and P can be given up to an arbitrary constant factor.

When we need to evaluate several expectation values, then the above choices of P_i force us to sample them separately. Many terms in the sum are however the same between different expectation values. We can make the algorithm more efficient by sampling all the expectation values in the same run. However, then we have to use only a single probability distribution $P(\mathbf{R})$. We have to ensure that $P(\mathbf{R})$ samples the big contributions of all expectation values. This can be done with $P(\mathbf{R}) = \sum_i P_i(\mathbf{R})$. With this compromise the rate of convergence is slower for the individual sums, but due to the more efficient evaluation of the various terms the overall time required to obtain the same accuracy will be reduced. This scheme has been used before to obtain the variance of the Hamiltonian along with the energy (*e.g.*, see Gros[54]) as follows

$$\begin{aligned}
\sigma_{\mathcal{H}}^2 &= \langle \mathcal{H}^2 \rangle - \langle \mathcal{H} \rangle^2 \\
\langle \Psi | \mathcal{H}^2 | \Psi \rangle &= \sum_{\mathbf{R}} \langle \Psi | \mathcal{H} | \mathbf{R} \rangle \langle \mathbf{R} | \mathcal{H} | \Psi \rangle \\
&= \sum_{\mathbf{R}} \frac{|\langle \mathbf{R} | \mathcal{H} | \Psi \rangle|^2}{P(\mathbf{R})} P(\mathbf{R}) \\
P(\mathbf{R}) &= \frac{|\langle \mathbf{R} | \Psi \rangle|^2}{\langle \Psi | \Psi \rangle}
\end{aligned} \tag{3.6}$$

While this is a fast way to obtain the variance as a byproduct, it also introduces a systematic error, since P is only appropriate for $\langle \mathcal{H} \rangle$. $\langle \Psi | \mathcal{H} | \mathbf{R} \rangle \langle \mathbf{R} | \mathcal{H} | \Psi \rangle$ need not be zero where $\langle \mathbf{R} | \Psi \rangle$ and therefore $P(\mathbf{R})$ vanishes. Since all of the terms in the sum are positive, $\sigma_{\mathcal{H}}$ will be underestimated. Also close to a node of $\langle \mathbf{R} | \Psi \rangle$, where $P(\mathbf{R})$ is small, the configuration space will not be sampled very often, even though — due to the small denominator — the corresponding term may be considerably off from the average and will therefore contribute substantially to the sum. All of this leads to an estimate for the variance which is smaller than the true value, and this discrepancy will not show up in the statistical error. We can test this systematic error by comparing with calculations done with a flat probability distribution $P(\mathbf{R}) = \text{const}$, which takes all terms into account with the same weight. From calculations for the t - J model on a system of 16 sites with 8 holes we conclude that the systematic error

is of the order of a few percent.¹ For bigger systems, where the slow convergence with the flat probability distribution forces us to use importance sampling, we can expect the nodes to become less important. Furthermore, the combined P used when evaluating many expectation values in the same run will counteract the systematic error. To get a quick qualitative estimate for the variance it is therefore reasonable to use Eq. (3.6).

3.3 Statistical Errors

As mentioned above the results obtained by Monte Carlo sampling are accurate only within a statistical error. This statistical error is also obtained from the same Monte Carlo data. In fact, the Monte Carlo data is analyzed analogously to experimental data.

The Metropolis algorithm generates a walk through configuration space. In general points along this walk which are close together are statistically dependent. A naive estimate would therefore lead to a statistical error which is too small. The statistical dependence can be measured with the autocorrelation function. The correlation between the data points will fall off exponentially with their distance and the statistical error can be corrected for. Another effect which has to be taken into account is that a Metropolis walk starting with an arbitrary configuration will not generate representative configurations for the first few steps.² To get reliable results we have to wait for a number of “warmup” steps before we start sampling.

In practice we calculate the statistical errors from completely independent runs using different random number generator seeds. This also allows us to perform the runs in parallel on different CPUs. One such run will then correspond to one “measurement” of the observables. If the runs have different length, this has to be taken into account by appropriate weights for the corresponding measurements. The number of terms in the Monte Carlo average can be used as the weight of the measurement.

Since we evaluate several expectation values in the same run, we have to consider the statistical dependence between different expectation values. This statistical dependence should not be confused with the statistical dependence mentioned before of one expectation value within a Monte Carlo run. The latter depends on the method to produce the random walks and is zero between different measurements, while the former is intrinsic to the expectation values. Let us label our expectation values with (x_1, \dots, x_N) . We perform M measurements which lead to the Monte

¹The energy converges to the same value with the flat probability distribution or with importance sampling as expected for this $P(\mathbf{R})$.

²This is much like a thermodynamic system starting away from equilibrium.

Carlo averages $(x_1^{(i)}, \dots, x_N^{(i)})$, $i \in \{1, \dots, M\}$. Let p_i be the weight of measurement i . If we then want to calculate a quantity $A = A(x_1, \dots, x_N)$, which depends on the observables x_n we have

$$\begin{aligned}
\bar{x}_n &= \frac{\sum_i p_i x_n^{(i)}}{\sum_i p_i} \\
\bar{A} &= A(\bar{x}_1, \dots, \bar{x}_N) \\
s_{\bar{A}}^2 &= \frac{1}{M-1} \frac{1}{\sum_i p_i} \sum_i p_i \left(\sum_n \frac{\partial A}{\partial x_n} (x_n^{(i)} - \bar{x}_n) \right)^2 \\
&= \sum_{n,n'} \left(\frac{\partial A}{\partial x_n} \right) \left(\frac{\partial A}{\partial x_{n'}} \right) \text{Cov}(x_n, x_{n'}) \\
\text{Cov}(x_n, x_{n'}) &= \frac{1}{M-1} \frac{\sum_i p_i (x_n^{(i)} - \bar{x}_n)(x_{n'}^{(i)} - \bar{x}_{n'})}{\sum_i p_i}
\end{aligned} \tag{3.7}$$

A result obtained by Monte Carlo is then quoted as $\bar{A} \pm s_{\bar{A}}$, where $s_{\bar{A}}$ corresponds to one standard deviation.

This scheme allows us to analyze the data separately from the Monte Carlo sampling. *E.g.*, we can investigate the t - J model for different J/t from the same set of data without losing any accuracy. All the information about the statistical error is contained in the covariance matrix $\text{Cov}(x_n, x_{n'})$.

For further information we refer to Numerical Recipes[57] or the ETH lecture notes by Gränicher[68]. These references also describe some statistical tests, which can be used to check whether all the statistical dependence has been taken care of properly. Such tests are useful to uncover some types of bugs in a program during program development.

3.4 Determinant Updates

Calculating the overlap of a RVB- or a Hartree-Fock wavefunction with a configuration involves the evaluation of a determinant. Many of the configurations are similar to each other, in that they have only a few electrons exchanged or moved to empty sites. The corresponding determinants differ only in a few rows and columns for an RVB wavefunction or columns only in the case of a Hartree-Fock wavefunction. *E.g.*, the Hamiltonians considered in this thesis, when applied to a configuration, will generate such a set of similar configurations. The corresponding set of determinants can be evaluated more efficiently than any one of them separately. Whereas the number of arithmetic operation needed to evaluate an $N \times N$ determinant scales as N^3 , the ratio of two determinants takes on the order of N operations if they differ only by a few rows (or only by a few columns) and on the order of N^2 operations if a few

rows and columns are changed. For one of the configurations the determinant and the inverse of the matrix have to be calculated beforehand. This, of course, requires again of the order of N^3 operations, but it has to be done only once for the whole set of configurations. Furthermore, the inverse for any one of the other matrices require $O(N^2)$ operations. In the random walk we can string together updates of determinants and inverses where each step requires $O(N^2)$ instead of the $O(N^3)$ operations. In their seminal paper Ceperley et al.[52] introduced this technique, which made variational Monte Carlo calculations feasible for fermions. They provide an explicitly formula for the determinant- and inverse-updates for one changed row (or column). If many rows and/or columns are changed, we can update by changing each of these rows and columns in turn. However, for configurations that don't lie on the way of the random walk (i.e., for the sampled terms in the evaluation of the expectation values) we don't need the new inverse nor any of the intermediate ones. It is then possible to combine all the updates, which reduces the operation count for the determinant update from $O(N^2)$ to the above mentioned $O(N)$ for rows (or columns) only. For changed rows and columns the determinant update still requires $O(N^2)$ operations, but there is a factor of at least 2 fewer operations needed compared with the inverse update.

In the following we give the for determinant update of M rows on one hand and of M rows and P columns on the other hand in a $N \times N$ matrix. We denote the old matrix with $[D_{old}]$ and the new matrix with $[D_{new}]$. The inverse of the old matrix is $[D_{old}^{-1}]$. The matrix elements are written as $[D_{old}]_{ij}$ and analogously for the others. The indices for the changed rows are i_1, i_2, \dots, i_M and if also columns are changed we use the indices j_1, j_2, \dots, j_P . For all other indices we have $[D_{old}]_{ij} = [D_{new}]_{ij}$.

Row update:

$$\begin{aligned}
q_{ii'} &= \sum_{k=1}^N [D_{new}]_{ik} [D_{old}^{-1}]_{ki'} \\
&\text{for } i, i' \in \{i_1, i_2, \dots, i_M\} \\
Q &= \det \begin{bmatrix} q_{i_1 i_1} & \cdots & q_{i_1 i_M} \\ \vdots & \ddots & \vdots \\ q_{i_M i_1} & \cdots & q_{i_M i_M} \end{bmatrix} \\
\det [D_{new}] &= Q \cdot \det [D_{old}]
\end{aligned} \tag{3.8}$$

Row and column update:

$$\begin{aligned}
s_{j,j'} &= \sum_{l=1}^N [D_{old}^{-1}]_{j,l} [D_{new}]_{lj'} \\
&\text{for } j \in \{1, 2, \dots, N\}, j' \in \{j_1, j_2, \dots, j_P\} \\
r_{i,j} &= \sum_{k=1}^N [D_{new}]_{ik} s_{kj} \\
&\text{for } i \in \{i_1, i_2, \dots, i_M\}, j \in \{j_1, j_2, \dots, j_P\} \\
q_{ii'} &= \sum_{k=1}^N [D_{new}]_{ik} [D_{old}^{-1}]_{ki'} \\
&\text{for } i, i' \in \{i_1, i_2, \dots, i_M\} \\
Q &= \det \begin{bmatrix} q_{i_1 i_1} & \cdots & q_{i_1 i_M} \\ \vdots & \ddots & \vdots \\ q_{i_M i_1} & \cdots & q_{i_M i_M} \end{bmatrix} \\
S_{j_\alpha j_\beta} &= Q^{-1} \det \begin{bmatrix} s_{j_\alpha j_\beta} & [D_{old}^{-1}]_{j_\alpha j_1} & \cdots & [D_{old}^{-1}]_{j_\alpha j_M} \\ r_{i_1 j_\beta} - [D_{new}]_{i_1 j_\beta} & q_{i_1 i_1} & \cdots & q_{i_1 i_M} \\ \vdots & \vdots & \ddots & \vdots \\ r_{i_M j_\beta} - [D_{new}]_{i_M j_\beta} & q_{i_M i_1} & \cdots & q_{i_M i_M} \end{bmatrix} \\
&\text{for } j_\alpha, j_\beta \in \{j_1, j_2, \dots, j_P\} \\
S &= \det \begin{bmatrix} S_{j_1 j_1} & \cdots & S_{j_1 j_P} \\ \vdots & \ddots & \vdots \\ S_{j_P j_1} & \cdots & S_{j_P j_P} \end{bmatrix} \\
\det [D_{new}] &= S \cdot Q \cdot \det [D_{old}]
\end{aligned} \tag{3.9}$$

With the interchange of rows and columns we obtain a complementary set of equations, which can be used to reduce the operation count depending on how many rows and columns are changed.

3.5 Efficient Reuse of Intermediate Results

Related to the last section there is another trick we can use to improve the performance of the program. Since we are sampling many expectation values at the same time and also due to the types of expectation values involved (*i.e.*, products of operators, which, *e.g.*, may hop an electron back and forth) we are generating the almost every configuration many times. We can make use of this fact in two ways: (1) we generate the configurations first and calculate the overlaps for every config-

uration once. This involves a considerable overhead for bookkeeping. We need to keep track where each configuration contributes. (2) we can store the overlaps with configurations already encountered in a table. For each new configuration we first consult the table to see whether there is already an entry. This second approach is considerably easier to implement, although the first might be slightly less demanding on memory requirements. The main point with using a table is to keep the time to access an element smaller than the time to evaluate the overlap. This is achieved by defining an order relation between any two configurations. The table can then be stored as a sorted list, or more efficiently as a binary tree. We find that using a binary tree reduces the access time considerably when the number of entries in the table becomes large. Another limitation is the memory used to store all the entries in the table. Even if a Monte Carlo run only generates a small fraction of all the configurations it is impractical or even impossible to store all configuration³ of one run. During the evaluation of the sampled terms the same configurations appear a few times shortly after each other and then they are almost never referenced anymore. This depends on the order in which the operators are evaluated. If we clear the table at the right moments during the evaluation of the expectation values we can reduce the memory consumption.⁴ For the cases we considered in this work we were able to reduce the number of times we had to evaluate an overlap by a factor of 5 to 10.

The essential point of this section is, that an algorithmic improvement like the one sketched here, typically leads to the most significant performance improvement. In this case it makes the method of the generalized Lanczos operators computationally feasible.⁵

3.6 Some Implementation Details

Every Monte Carlo method uses a random number generator. If this generator is of bad quality, the results from the Monte Carlo program might be questionable. Some of the random number generators provided in the standard libraries are known to be of poor quality. Furthermore, they are different between different machines, so that tests of the program could not be repeated in exactly the same way on a new machine. In this work we used the implementation “ran1” from the *Numerical*

³The dimension of the Hilbert space for the 50 sites lattices with a few holes considered in this work is on the order of $10^{18} \dots 10^{22}$.

⁴This will also reduce the access time due to the smaller tables.

⁵In the standard Variational Monte Carlo calculations there are much fewer operators involved and the generated configurations can in general be organized quite trivially so that each overlap has to be evaluated only once.

Recipes in C[57], first edition,⁶ which is expected to be of good quality and which can be used on any machine as the source code is available. Our results are therefore at most valid to the extent that “ran1” shows no statistical correlations. The second edition of *Numerical Recipes* discusses the possibility to use “sub-random” instead of “(pseudo-)random” numbers to speed up the convergence from the typical $O(N^{1/2})$ one gets from a Monte Carlo algorithm. For our case this would involve finding a walk through configuration space that would cover more and more of configuration space when the number of configurations get bigger without clustering in any region. Finding such a walk is non-trivial as it depends on the structure of configuration space. Also “stratified sampling” instead of or in addition to importance sampling depends on how to divide up configuration space in order to make use of correlations. In this work we have not attempted to use such schemes. Although, such schemes may be possible for the lattices considered here, they will in general be more advantageous in continuous systems.

Except for the evaluation of the sampled terms in each step the order of the instructions in a Monte Carlo program cannot be predicted at the time the program is written. Consequently, a typical Monte Carlo program will vectorize only poorly. However, many runs starting with different random seeds can be performed in parallel. The runs are completely independent of each other and use relatively little memory. These are ideal condition for using a parallel computer. In this work we used a network of 30 workstations with a total computing power on the order of 80 MFlops. The runs were automatically distributed by a batch system which attempted to make the most efficient use of the available CPUs[69].

As with any program a Monte Carlo program needs to be tested. The usual kind of checks, *i.e.*, running a number of independently verified test cases, will uncover some bugs. However, a program based on a random number generator will necessarily generate results with statistical scatter. A subtle bug, like missing one out of many iterations of a loop (usually the first or the last iteration), may produce an error of the same order or smaller than the statistical scatter. It is therefore essential to design the implementation in a modular way, where each module can be tested independently. This is especially important for the performance improvements discussed in this chapter, which introduce another level of complexity. In this work we use the object-oriented programming language C++ for the implementation[70].

⁶Some of the random number generators in *Numerical Recipes* were changed in the second edition. This includes “ran1”.

Chapter 4

The Heisenberg Model

Even though the Heisenberg model is one of the oldest and simplest non-trivial models in many particle quantum mechanics, only a few results are rigorously known. The model is defined by the Hamiltonian

$$\mathcal{H} = J \sum_{\langle i,j \rangle} \mathbf{S}_i \cdot \mathbf{S}_j \quad (4.1)$$

The interaction is between pairs of spins- $\frac{1}{2}$ connected via nearest-neighbor bonds with $J > 0$. The model can also be generalized to higher spins S . For large enough S the spins behave classically and the groundstate is antiferromagnetically ordered. It should be noted that the ferromagnetic case with $J < 0$ is very different from the antiferromagnetic case. For ferromagnetic coupling the groundstate is degenerate and corresponds to the subspace of maximal spin. The excited states are well described by spin wave theory.

For antiferromagnetic coupling the fully antiferromagnetically ordered Néel state is not an eigenstate of the Hamiltonian and therefore not the groundstate. It is not a priori clear whether the quantum fluctuations would completely destroy long-range order. In one dimension the Bethe ansatz[71] solves the spin- $\frac{1}{2}$ antiferromagnetic Heisenberg chain exactly. It shows that the groundstate of the Heisenberg model has no antiferromagnetic long-range order in one dimension. In three dimensions it is known that for all spins[72, 73] there is antiferromagnetic long-range order below a finite critical temperature and hence in the groundstate. For the two-dimensional case we know that there is no long-range order at finite temperature[4]. A finite long-range order in the groundstate (*i.e.*, at $T = 0$) has only been shown for $S \geq 1$ [74] and for spin- $\frac{1}{2}$ with enough anisotropy[75, 76]. To date no rigorous result is known, which would prove the existence or non-existence of antiferromagnetic long-range order of the *isotropic* spin- $\frac{1}{2}$ antiferromagnetic Heisenberg model on a two-dimensional square lattice. One of the few exact known results is given by the Marshall-sign rule, which implies a singlet groundstate on a bipartite lattice[77, 78].

Despite the lack of rigorous results the evidence from numerical calculations ranging from exact diagonalization[79, 80, 81] and Green's function Monte Carlo[82, 83] to spin wave theory[84, 85, 86] and series expansions[87, 88, 89, 90] clearly show finite long-range order in the groundstate which is reduced by 40% compared with the Néel state. Furthermore, variational Monte Carlo studies favor antiferromagnetic long-range order, although they are less reliable in estimating the magnitude of the order[91, 92, 93, 94, 95].

As the spin- $\frac{1}{2}$ Heisenberg antiferromagnet naturally describes the CuO_2 planes of the undoped parent compounds of the High T_c materials, there has been renewed interest in recent years. An overview over the presently known results can be found in the review by Manousakis[96].

4.1 The Heisenberg Model as a Test Case

The spin- $\frac{1}{2}$ antiferromagnetic Heisenberg model can serve as an ideal test case for our method. Apart from the fermionic description, where an electron with spin $\frac{1}{2}$ is placed at each lattice site, there is an equivalent bosonic description. The bosonic nature of the problem allows the use of quantum Monte Carlo techniques without the fermion sign problem. We can then compare our results using the fermionic description to the numbers obtained from the equivalent bosonic system. While for the Heisenberg model the fermionic description is unnecessary, other fermionic problems cannot be mapped to an equivalent bosonic model. Before we use our method on such a system we want to test it for a case where reliable results obtained independently are available as is the case for the Heisenberg model.

The bosonic description starts from the completely antiferromagnetically ordered Néel state. The spin-flip operators S_i^+ and S_i^- are associated with the appropriate creation and annihilation operator a_i^\dagger and a_i on each sublattice. These creation and annihilation operators then observe the usual commutation relations for bosons with the additional constraint that there can be no more than one boson at each site, *i.e.*, they are hard-core bosons. For general spin S the bosons are defined by a generalization of the Holstein-Primakoff transformation[97] for antiferromagnets which leads to the spin-wave theory for antiferromagnets[84]. An overview over the Holstein-Primakoff transformation and the resulting spin-wave theory can also be found in Manousakis[96].

The most reliable values for the groundstate energy can be obtained by quantum Monte Carlo methods. Although they use different projection and guiding functions in their Green's function Monte Carlo calculations, Trivedi *et al.*[82] and Carlson[83] obtain both a value of -0.6692 ± 0.0002 per site, or -0.3346 ± 0.0001 per bond. These

values compare well to other methods like spin-wave theory or series expansion[90]. Due to finite size scaling, the groundstate energy for the 50 sites lattice that we will investigate below has a lower value of ≈ -0.3375 per bond[82].

The antiferromagnetic long-range order is characterized by the staggered magnetization $m^\dagger = (1/N) \sum_{\mathbf{r}} (-1)^{r_x+r_y} \langle S_{\mathbf{r}}^z \rangle$ measured with a small staggered magnetic field $h(\mathbf{r}) = (-1)^{r_x+r_y} h$. To obtain the staggered magnetization of the groundstate, the thermodynamic limit has to be performed before letting $h \rightarrow 0$. This difficulty can be avoided by extracting m^\dagger from the staggered spin-spin correlation.

$$C_{spin}(\mathbf{R}) = (-1)^{R_x+R_y} \frac{1}{N} \sum_{\mathbf{r}} \langle \mathbf{S}_{\mathbf{r}} \cdot \mathbf{S}_{\mathbf{r}+\mathbf{R}} \rangle \quad (4.2)$$

$$m^{\dagger 2} = C_{spin}(\infty) \approx C_{spin}(\mathbf{R}_{max}) \quad (4.3)$$

where \mathbf{R}_{max} is the longest possible distance in a finite lattice with periodic boundary conditions.

The staggered magnetization is more difficult to obtain reliably from Green's function Monte Carlo. Since it does not commute with the Hamiltonian, its value is more sensitive to the choice of the guiding wavefunction. Trivedi *et al.*[82] report a value of $m^\dagger = 0.31 \pm 0.02$ while the value of Carlson[83] is 0.34 ± 0.01 . This indicates a value of the staggered magnetization, which is reduced by 30%...40% with respect to the Néel state. While exact diagonalization tends to favor a lower value for m^\dagger [80], the series expansions agree quite well with this value[89, 90].

The staggered magnetization m^\dagger does not commute with the Hamiltonian. It is therefore not a conserved quantity and the groundstate is a mixture of states corresponding to different m^\dagger . It is then possible to find variational states with low energy, which have zero staggered magnetization. Liang *et al.*[98] have found such a state using a resonant valence bond wavefunction. This shows that the energy alone is not a good enough criterion to obtain information about other properties of the groundstate using purely variational approaches.

4.2 Variational Monte Carlo with Lanczos Iterations

Standard variational Monte Carlo has been used successfully to model the antiferromagnetic correlations in the t - J model (*e.g.*, see Yokoyama and Shiba[92], Chen *et al.*[44], or Gros[54]). We will use the same wavefunction as Gros with the same parameters as our starting point for the Lanczos iterations¹. This wavefunction combines spin-density wave orbitals into a d-wave BCS-type condensate. This leads to

¹Results of this chapter have also been published in Ref. [99]

an RVB ansatz which mixes singlet and triplet bonds. The wavefunction is defined as[54, 44]

$$\begin{aligned}
|\Psi_0(\Delta_{\text{AF}}, \Delta_{\text{SC}})\rangle &= \mathcal{P}_G \mathcal{P}_N \prod_{\mathbf{k} \in \text{BZ}} (u_{\mathbf{k}} + v_{\mathbf{k}} d_{\mathbf{k},\uparrow}^\dagger d_{-\mathbf{k},\downarrow}^\dagger) |0\rangle \\
\begin{pmatrix} d_{\mathbf{k},\sigma}^\dagger \\ d_{\mathbf{k}+\mathbf{Q},\sigma}^\dagger \end{pmatrix} &= \begin{pmatrix} a_{\mathbf{k}} & \sigma b_{\mathbf{k}} \\ -\sigma b_{\mathbf{k}} & a_{\mathbf{k}} \end{pmatrix} \begin{pmatrix} c_{\mathbf{k},\sigma}^\dagger \\ c_{\mathbf{k}+\mathbf{Q},\sigma}^\dagger \end{pmatrix} \\
a_{\mathbf{k}} = \cos(\theta_{\mathbf{k}}), \quad b_{\mathbf{k}} = \sin(\theta_{\mathbf{k}}), \quad \cos(2\theta_{\mathbf{k}}) &= \epsilon_{\mathbf{k}} / \sqrt{\epsilon_{\mathbf{k}}^2 + \Delta_{\text{AF}}^2} \\
v_{\mathbf{k}}/u_{\mathbf{k}} = \Delta_{\mathbf{k}} / \left(\epsilon_{\mathbf{k}} + \sqrt{\epsilon_{\mathbf{k}}^2 + \Delta_{\mathbf{k}}^2} \right) \\
\Delta_{\mathbf{k}} = \Delta_{\text{SC}}(\cos(k_x) - \cos(k_y)) \\
\epsilon_{\mathbf{k}} = -2(\cos(k_x) + \cos(k_y))
\end{aligned} \tag{4.4}$$

where \mathcal{P}_G and \mathcal{P}_N are the Gutzwiller and N -particle projectors, respectively. The operators $d_{\mathbf{k},\sigma}^\dagger$ create an electron in a spin-density wave orbital controlled by Δ_{AF} . The Cooper-pairs are condensed with a d-wave symmetry controlled by the gap Δ_{SC} . For other symmetries we have to substitute for the appropriate gap function $\Delta_{\mathbf{k}}$.

When the spin-density wave gap Δ_{AF} is zero, the wavefunction is a singlet RVB state and has no long-range order, *i.e.*, the staggered magnetization vanishes in the thermodynamic limit. Any finite value of Δ_{AF} will lead to a finite staggered magnetization but will also mix in some triplet and higher excited spin states. It should be noted that also for $\Delta_{\text{AF}} = 0$ long-range bonds still have a considerable weight, so that for the finite size lattice considered here there is a considerable antiferromagnetic correlation even at the largest distance available.

Since the groundstate is known to be a singlet[77, 78], we would ideally want to have this state projected onto the singlet subspace (for finite Δ_{AF}). However, this would increase the computing time. In the simplest case, for a Slater determinant, there is a factor of $N + 1$ increase in computing time, where N is the number of spins. For a more general wavefunction, like the RVB ansatz given above, the number of term generated by the singlet projection operator rises exponentially with the number of spins. Therefore we do not attempt to perform the singlet projection for the wavefunction (4.4). Although, we can expect the influence of the triplet and higher excited spin states to be negligible for small enough Δ_{AF} we have to be careful in the interpretation of the results obtained with a finite Δ_{AF} .

Gros has shown that a lower energy is obtain by choosing a finite spin-density wave gap Δ_{AF} . This is consistent with a groundstate with finite staggered magnetization. Furthermore Gros has shown that for this state the variance of the Hamiltonian is smallest for the optimal energy. This is a strong indication that the

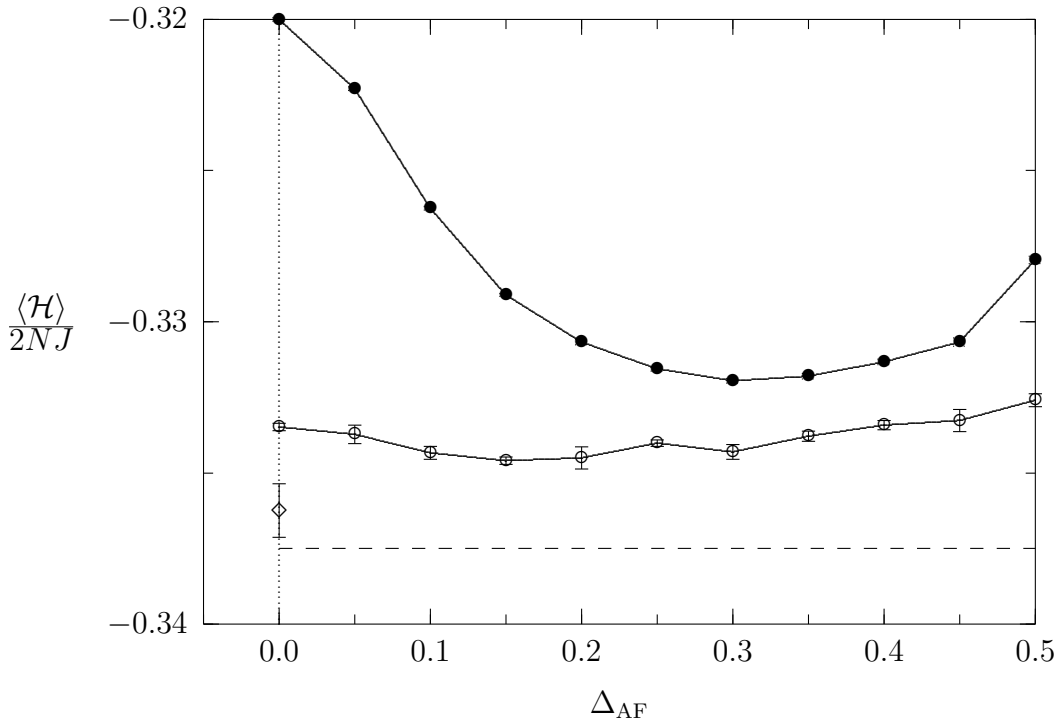


Figure 4.1: Energy expectation values of the Heisenberg Hamiltonian normalized by the number of bonds on a 50 sites lattice. The energies are shown as a function of the variational parameter Δ_{AF} while Δ_{SC} was held fixed at 0.5. The upper curve (\bullet) shows the energy as obtained by standard VMC, in agreement with Gros, while the lower curve (\circ) shows the improved energies after one Lanczos iteration. For the case of $\Delta_{AF} = 0$ a second Lanczos step has been carried out. The result is shown as \diamond . The dashed line indicates the expected ground state energy as reported from GFMC calculations by Trivedi *et al.* and Carlson.

wavefunction closely models the groundstate.

We can now perform Lanczos iterations on this wavefunction, which will yield variational states with a lower energy. The energy obtained in this way is shown in Fig. 4.1. We fixed the d-wave gap at $\Delta_{SC} = 0.5$, while the spin-wave gap was varied in an interval $\Delta_{AF} = 0.0 \dots 0.5$. The points indicated with \bullet correspond to the values obtained before the Lanczos iterations. They are in agreement with the results from Gros. After one Lanczos iteration we obtain the values denoted by \circ . We can see that the relative improvement is biggest for the singlet state at $\Delta_{AF} = 0$. For this state we carried out a second Lanczos iteration with the result shown as \diamond . The values of the energy for the singlet variational wavefunction with $\Delta_{SC} = 0.5$ and $\Delta_{AF} = 0$ are -0.32000(6) before, -0.33348(12) after the first, and -0.33625(89) after the second Lanczos iteration. These are energies per bond measured in units of the coupling constant J . The value of the second Lanczos iteration is the lowest value obtained in this work and is lower than other reported variational bounds[96].

It is a well known fact in exact diagonalization that taking symmetry into consid-

eration leads to faster convergence of the Lanczos method. For a well enough chosen initial wavefunction one needs about as many Lanczos steps to achieve convergence as there are eigenstates with non-negligible overlap with the initial wavefunction. After that many steps, the constructed set of states essentially spans the same Hilbert space as do these eigenstates. If the groundstate has a considerably smaller weight than some other eigenstates, the Lanczos algorithm will first try to converge to the lowest of those excited states, before the groundstate can take over. Projecting onto a symmetry of the groundstate will therefore reduce the dimension of the effective Hilbert space and at the same time lower the probability of having an excited state screening the groundstate. This problem will even be more prominent in our method, as we can do only a few iterations. Using the variance of the Hamiltonian we can tell whether the current Lanczos step brought us closer to an eigenstate or merely shifted the weight from higher to lower energy eigenstates. While in the first case the variance is reduced, it may get bigger in the second case. As the sequence approaches the groundstate, the variance converges to zero, as discussed in section 2.1. For our trial wavefunctions we observe that $\sigma_{\mathcal{H}} = \langle (\mathcal{H} - \langle \mathcal{H} \rangle)^2 \rangle^{1/2}$ is reduced by a factor of about 2 in one Lanczos step. The numerical values for the initial wavefunction with $\Delta_{\text{SC}} = 0.5$ and $\Delta_{\text{AF}} = 0.0$ again measured per bond in units of J are 0.02725(22) before, 0.01463(98) after the first, and 0.00844(772) after the second Lanczos iteration.

The important effect that the symmetry of the initial trial wavefunction has on convergence, is illustrated by the bigger improvement in energy as Δ_{AF} approaches 0. For smaller values of Δ_{AF} the higher spin components are more and more suppressed until $\Delta_{\text{AF}} = 0$ gives a pure spin singlet state. To confirm this observation, we have also evaluated the energy expectation values for the pure d-wave state as a function of Δ_{SC} as well as the pure SDW state as a function of Δ_{AF} . When we compare all these results again with the expected groundstate energy of $-0.3375J$ from Green's function Monte Carlo, we observe the spin singlet wave functions to recover between 70 and 80 % of the difference, whereas this value drops well below 50 % when Δ_{AF} is turned on even only to moderate values. The singlet case continues to show a big relative improvement also for the second Lanczos iteration, as shown in Fig. 4.1.

As mentioned above, Δ_{AF} is not a direct measure for the antiferromagnetic order. It is merely a variational parameter, which together with Δ_{SC} determines the spin order. The antiferromagnetic order will extend over a considerable range depending on Δ_{SC} even when $\Delta_{\text{AF}} = 0$. After the Lanczos iteration the variational parameters are even more meaningless, since the wavefunction is changed by the iteration. In order to obtain some information about the spin order, one has to measure the correlations directly. This will be shown in the next section. It is also important

to notice that a low energy of the initial wavefunction alone is not good enough as a criterion to find a good starting wavefunction. Choosing a wavefunction from a sector of the Hilbert space with the right quantum numbers for the groundstate is more important. We therefore find that although the introduction of Δ_{AF} lowers the energy in the standard variational Monte Carlo, it is important *not* to use (a finite) Δ_{AF} for the Lanczos iterations.

4.3 Spin Order

Additionally to the energy and variance, we can measure the spin-spin correlation $C_{spin}(\mathbf{R}) = (-1)^{R_x+R_y} \frac{1}{N} \sum_{\mathbf{r}} \langle \mathbf{S}_{\mathbf{r}} \cdot \mathbf{S}_{\mathbf{r}+\mathbf{R}} \rangle$ of the variational wavefunction before and after the Lanczos iteration. This will give us direct information about the spin order and how the Lanczos iteration changes it when converging towards the groundstate. For the singlet case of $\Delta_{\text{SC}} = 0.5$ and $\Delta_{\text{AF}} = 0$ which we have found to be the optimal choice for the Lanczos iterations Fig. 4.2 shows the results for the z -component of the spin-spin correlation function. We need to multiply this value by 3 to obtain the total spin-spin correlation.² The value for the staggered magnetization is therefore $m^\dagger = (3 |\langle S_i^z S_{i+\mathbf{R}_{max}} \rangle|)^{1/2}$.

The d-wave state has an antiferromagnetic order which decays as a power law. Even though this would lead to zero staggered magnetization in the thermodynamic limit $C_{spin}(\mathbf{R})$ remains quite large at all distances for the 50 sites lattice considered here. This suggests that it is the slow decay which is responsible for the low variational energy. The Lanczos iteration confirms this expectation as it enhances the spin-spin correlation at all distances.

In the following table we compare our results with the Green's function Monte Carlo data by Trivedi and Ceperley[82, 100] and Carlson[83].

Trivedi and Ceperley[82]	Carlson[100]	Standard VMC	VMC + Lanczos
0.31 ± 0.02	0.34 ± 0.01	0.29	0.34

The values from the Green's function Monte Carlo are extrapolated to the thermodynamic limit. For smaller systems these values are higher. Spin-wave theory predicts a finite size dependence of the staggered magnetization of

$$m^\dagger(L) = m^\dagger(\infty) + \mu L^{-1} + \dots \quad (4.5)$$

where L is the linear dimension. This dependence should also be reflected in the distance dependence of $C_{spin}(\mathbf{R})$ for the larger distances. For the 50 sites lattice

²This is only possible for a singlet state. For the general case the x - and y -components have to be evaluated separately. Since they are non-diagonal, this would increase the overall computing time.

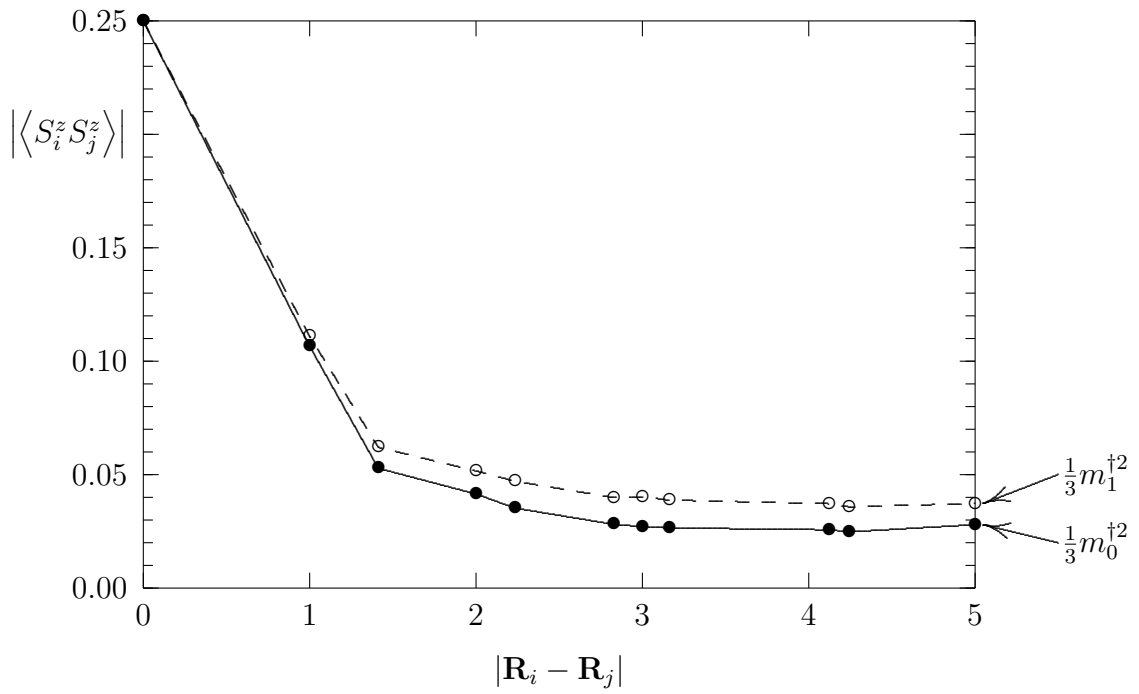


Figure 4.2: z component of the staggered spin-spin correlation as a function of distance. Shown are the values before (●) and after (○) the first Lanczos iteration for a d-wave RVB state ($\Delta_{\text{SC}} = 0.5, \Delta_{\text{AF}} = 0$, see text). The values at the largest distance are used for an estimate of the staggered magnetization.

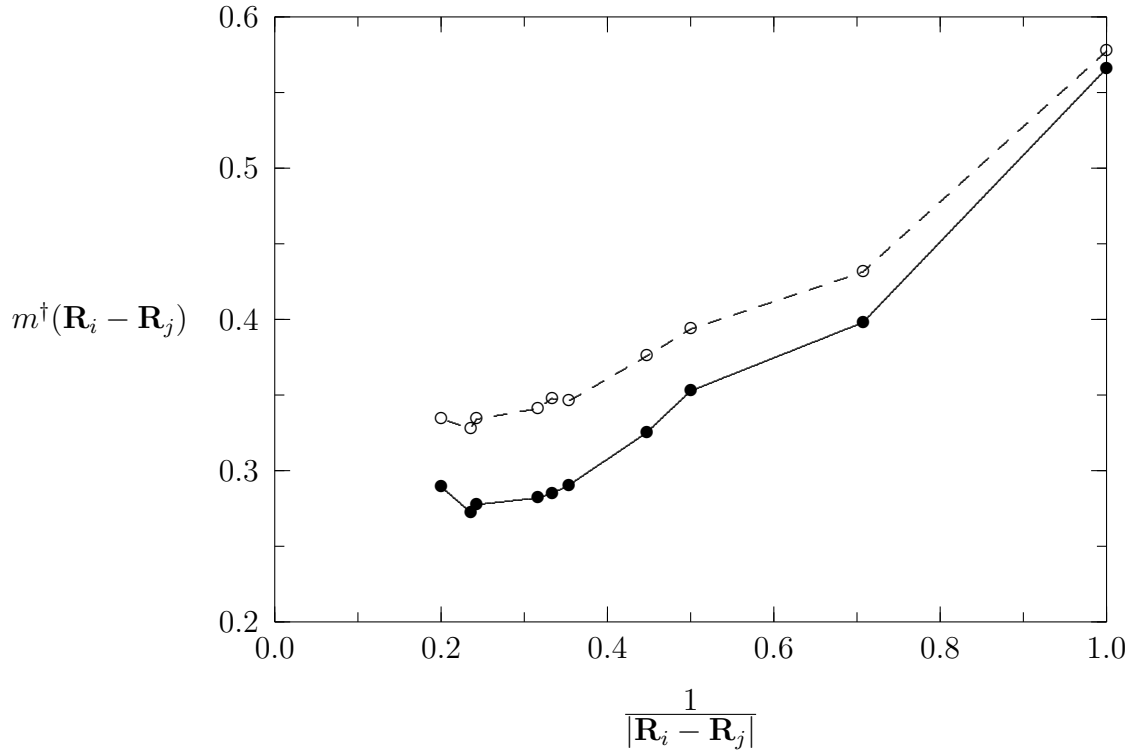


Figure 4.3: Staggered magnetization as a function of inverse distance for the 50 sites lattice. Spin-wave theory predicts a linear dependence on inverse distance. The thermodynamic limit of the staggered magnetization corresponds to the limit $\frac{1}{\Delta \mathbf{R}} \rightarrow 0$. ● are the values before and ○ are after the Lanczos iteration.

we show in Fig. 4.3 the same data as in Fig. 4.2 represented to reflect this distance dependence. The 50 sites lattice does not allow a reliable extrapolation to the thermodynamic limit. Nevertheless, the values after the Lanczos iteration is in qualitative agreement with $m^\dagger = 0.3 \dots 0.32$ which is expected for the staggered magnetization in the thermodynamic limit from other calculations[96].

4.4 Conclusions

In this chapter we have shown that the Lanczos iteration is a valuable tool to construct an unbiased improvement for a given wavefunction. This will not only improve the variational upper bound for the energy, but we can also get some information about other observables. In particular we have shown that with the Lanczos iteration the staggered magnetization tends to approach the value expected for the groundstate. It should also be noticed that these calculation were performed using the fermionic representation of the Heisenberg model. The value we obtain for the energy is considerably better than typical values obtained for the fermionic description[96]. This allows us to use the presented method for other fermionic models without the limitations given by the sign problem.

These calculations also show the limitations of a straightforward application of the Lanczos method to the variational Monte Carlo approach. While the first Lanczos iteration can easily be handled with the presently available computing power — it could even be used for slightly larger lattices — every additional Lanczos step leads to an exponential rise in the necessary computing time. For 50 sites we cannot go beyond the second Lanczos step, except for some special wavefunctions like the Vandermonde determinants in one dimension.

In the first Lanczos iteration the spin configuration on each nearest neighbor bond are optimized (with the energy as the criterion). The second iteration will again optimize the spin configuration on a nearest neighbor pair, but this second pair can be in any relative position to the first one. This leads to the exponential increase in the number of terms. However, not all relative positions of the bonds in the higher order Lanczos steps lead to an equally important contribution in the improvement of the energy. The lattice- and spin-symmetry determines only a few coefficients in the terms. With generalized Lanczos operators, as discussed in section 2.4, we can therefore improve the variational wavefunction further without the exponentially increased time requirements. We will make use of such generalized Lanczos operators in the investigation of the t - J model, where the Hilbert spaces are considerably larger.

Chapter 5

The t - J Model

As noted in chapter 1 the t - J model is one of the simplest yet promising models to describe the high- T_c cuprates. Various investigations have shown that the ground-state can exhibit different phases depending on the two parameters hole density δ and coupling strength J/t .¹ The $T = 0$ phase diagram provides a convenient way to represent the regions in parameter space where a particular phase is realized in the groundstate. Apart from specific predictions for an experiment (like susceptibility measurements or photoemission), considerable effort has been devoted the determination of this phase diagram. A few phases have been successfully identified and are summarized in the review by Dagotto[5] as shown in Fig. 5.1.

The phase separation at large J is well established. After being conjectured by Emery *et al.*[32] from exact diagonalizations of a 4×4 cluster, the phase separation boundary was then determined from high-temperature expansion directly for the thermodynamic limit by Putikka *et al.*[34]. It is still unclear which is the lower critical value of J for which phase separation occurs (in the region of small δ). While Emery *et al.* estimated that phase separation is possible for any value of J whenever δ is small enough, the high-temperature expansion clearly showed a finite critical value J_c below which there is no phase separation. Recently, Prelovšek and Zotos[36] investigated the arrangement of the holes in more detail using finite size clusters. They find that 4 holes bind into two well separated pairs for $J > J_c \sim 0.2t$. Only at couplings of $J > J_s \sim 1.5t$ they find that the pairs attract each other. However, even then they do not form a compact cluster. Prelovšek and Zotos find that the 4 holes arrange predominantly on a line in the $(1, 0)$ direction. They argue that in the thermodynamic limit this will lead to domain walls and consequently to the existence of a so-called “striped phase”. This striped phase would be an incommensurate charge density wave (CDW) and spin density wave (SDW) structure. Only at much larger couplings ($J > J_s^* \sim 2.5t$) they find that the holes form a compact cluster,

¹Since $J < t$ is expected for the cuprates, energies are conveniently measured in units of t , *i.e.*, the kinetic energy.

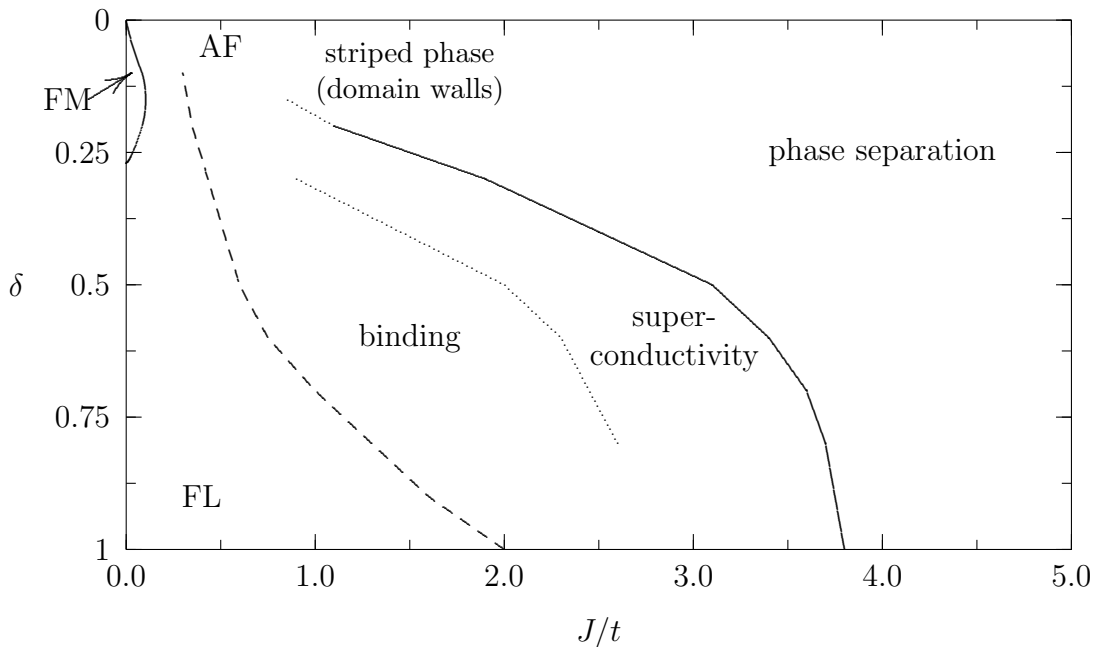


Figure 5.1: Phase diagram as compiled by Dagotto. AF denotes antiferromagnetism, FM ferromagnetism, and FL indicates the region of a Fermi liquid at low electron density. The different phases are discussed in the text.

which one would expect for the phase separated state. These studies indicate that the transitions from the homogeneous to the phase separated state is more involved than what the earlier investigations assumed.

Experimentally, evidence for phase separation has been found in the oxygen enhanced compound $\text{La}_2\text{CuO}_{4+\delta}$ [101, 102, 103]. However, it is not clear how much of this effect is due to the mobile ions present in the material. It is then questionable whether the t - J model still provides an accurate description for such a material. Other energies may become comparably important as the nearest neighbor interactions between the electrons. For other compounds no signs of phase separation have been observed to date.

The half filled case ($\delta = 0$) corresponds to the Heisenberg antiferromagnet, where long-range antiferromagnetic order is expected. For finite doping one can expect the antiferromagnetic order to persist to some extent (denoted by AF in the phase diagram Fig. 5.1). This is especially true for the phase separated region where one of the phases corresponds to the half filled case. Also for striped phases one expects the spins between the domain walls to align antiferromagnetically. This may restrict the antiferromagnetic order to be short-range and lead to incommensurate order. It is unclear how far the antiferromagnetism extends into the region of finite doping and how relevant it is to the superconducting state. Nevertheless, antiferromagnetically correlated spins are successfully used to explain experiments related to magnetic properties[104].

For low values of $J < 0.1t$ high-temperature expansion[30] and exact diagonalization[31] have found a region of ferromagnetic correlations shown as FM in the phase diagram Fig. 5.1. Although this region is fairly well established, the parameters in the cuprates are most likely outside of its range.

The regions in the phase diagram indicated by “superconductivity” and “binding” have the biggest uncertainties. The boundaries for these regions are qualitative estimates mainly based on calculations on a 4×4 cluster[40]. The only strong signal for superconducting correlations in such a small system is obtained for quarter filling where enough charge carriers are present to form a condensate. The difference between “binding” and “superconductivity” is then only a qualitative estimate indicative of the strength of the static structure factor corresponding to the d-wave pair-pair correlation function. A recent investigation of the anomalous Green’s function by Ohta *et al.*[41] including calculations up to an 18 sites cluster has also shown a finite d-wave gap which they estimated to be proportional to J (*i.e.*, they don’t find a critical J below which there is no superconductivity). For calculations on such small clusters one has to keep in mind that the shell effects are considerable.² As shown in section 2.8 for a finite lattice there are only a finite number of corresponding \mathbf{k} -points in the Brioullin zone of the reciprocal lattice. Due to the symmetry 4 of the \mathbf{k} orbitals will be degenerate except for points like $\mathbf{k} = 0$ which lie on special symmetry lines. For fillings where such a set of 4 \mathbf{k} orbitals is not completely occupied or empty this leads to a degeneracy. Correlations like superconductivity might lower the energy in order to remove the degeneracy even when this is not the case in the thermodynamic limit. One should therefore expect variations of the results with the number of electrons with a period of 8.

Strong support for superconductivity also comes from variational calculations. Typically, these calculations tried to estimate the relative stability of antiferromagnetic versus superconducting order[44, 27, 45]. The variational Monte Carlo method allows larger systems to be investigated and the results therefore have more relevance for the thermodynamic limit³ than the small systems used for exact diagonalization mentioned above.

As can be seen in the phase diagram Fig. 5.1, many different phases compete in the region of parameters relevant to the cuprates ($\delta < 0.5$, $J/t \approx 0.3 \dots 0.4$). This delicate balance between various instabilities may explain in part why so few reliable results are available. It also points to a problem with variational approaches. The bias introduced by the choice of the wavefunction cannot easily account for the

²Shell effects are also considerable for bigger lattices. However, for such small systems there is only one closed shell configuration with 10 electrons.

³This is especially true for the wavefunctions considered, which scale well with the system size

small differences in energy of the various groundstates, which are possible. In what follows we will eliminate much of this bias using the generalized Lanczos operators introduced in section 2.6.

5.1 Energy and Variance

The most important quantities in a variational calculation are the energy and the variance[54] as discussed in section 2.1. Using this criterion with the generalized Lanczos operators we obtain an improved upper bound for the groundstate energy. Additionally we can compare the variances before and after applying the generalized Lanczos operators. If the variance increases for a Lanczos iteration then the starting wavefunction was closer to an excited eigenstate and the iteration redistributed the weight from higher to lower energies. This allows us to judge the quality of the starting wavefunction to some extent.⁴

The t - J Hamiltonian was given in Eq. 1.2. The variational wavefunctions correspond to a condensate of d-wave Cooper-pairs with a short correlation length as follows

$$\begin{aligned}
 |\Psi_0(D, \mu)\rangle &= \mathcal{P}_G \mathcal{P}_N \prod_{\mathbf{k} \in \text{BZ}} (u_{\mathbf{k}} + v_{\mathbf{k}} c_{\mathbf{k}, \uparrow}^\dagger c_{-\mathbf{k}, \downarrow}^\dagger) |0\rangle \\
 v_{\mathbf{k}}/u_{\mathbf{k}} &= \Delta_{\mathbf{k}} / \left(\epsilon_{\mathbf{k}} + \sqrt{\epsilon_{\mathbf{k}}^2 + \Delta_{\mathbf{k}}^2} \right) \\
 \Delta_{\mathbf{k}} &= D(\cos(k_x) - \cos(k_y)) \\
 \epsilon_{\mathbf{k}} &= -2t(\cos(k_x) + \cos(k_y)) - \mu
 \end{aligned}
 \tag{5.1}$$

This wavefunction was also considered by Li *et al.*[45] where they investigated various symmetries for $\Delta_{\mathbf{k}}$. Chen *et al.*[44] and Giamarchi and Lhuillier[27] also included some long-range antiferromagnetic order characterized by a SDW gap as in Eq. 4.4. Because this would mix in triplet and higher excited spin states and thus lower the symmetry, it leads to slower convergence of the Lanczos iterations as observed for the Heisenberg case in section 4.2. Furthermore the variational calculations have found that the SDW gap is quickly suppressed with doping. We will therefore concentrate on the wavefunction Eq. 5.1. The variational wavefunction allows us to control the long-range d-wave order via the gap parameter D . For the \mathbf{k} -points where $\Delta_{\mathbf{k}}$ has a node the ratio $v_{\mathbf{k}}/u_{\mathbf{k}}$ is not well defined when $\epsilon_{\mathbf{k}} < 0$. In the thermodynamic limit the nodes of $\Delta_{\mathbf{k}}$ in the Brillouin zone are negligible. The effect of these nodes on the wavefunction accounts for much of the finite size effects. Due to the tilted periodic boundary conditions the 50 sites lattice which we will use has only one

⁴We have indeed found some cases where the wavefunction had to be rejected due to the variance criterion even though the energy would have a good value. The wavefunctions shown in the results fulfill both criteria.

point with $\Delta_{\mathbf{k}} = 0$ (at $\mathbf{k} = 0$) and is thus an optimal choice to reduce the finite size effects (see Fig. 2.1). Since $\mathbf{k} = 0$ is deep inside the Fermi sea we set $v_{\mathbf{k}=0} \rightarrow 1$ and $u_{\mathbf{k}=0} \rightarrow 0$ which leads to a ratio $v_{\mathbf{k}}/u_{\mathbf{k}} \rightarrow \infty$. In an actual calculation we choose a large but finite ratio. For $D \rightarrow 0$ the choice of this ratio has a bigger influence on the wavefunction and the Fermi sea will be defined as the extrapolation from small but finite values of D .⁵

Whereas the long-range order is fixed by construction, there is essentially no control over the short-range behavior of the wavefunction. This is taken care of by the generalized Lanczos operators. Here we use the most general operator which is compatible the spin and lattice symmetry and which has the same characteristic length scale as the Hamiltonian, *i.e.*, it acts on nearest neighbor bonds.

$$\mathcal{A} = \alpha_0 + \alpha_1 \sum_{\langle i,j \rangle, \sigma} (\tilde{c}_{i,\sigma}^\dagger \tilde{c}_{j,\sigma} + \text{h.c.}) + \alpha_2 \sum_{\langle i,j \rangle} \mathbf{S}_i \cdot \mathbf{S}_j + \alpha_3 \sum_{\langle i,j \rangle} \frac{1}{4} n_i n_j \quad (5.2)$$

5.1.1 Quarter Filling

We can test our method for the 4×4 cluster where exact results are available[105]. In Fig. 5.2 we show the energy in units of t for quarter filling. For 16 sites this corresponds to 8 holes, whereas for 50 sites we choose 24 holes so as to have an even number of holes for the RVB wavefunction.

In Fig. 5.2 the line labeled “RR” denotes the energy expectation value obtained by standard variational Monte Carlo. This energy expectation value is taken for a wide variety of different variational gap parameters D in Eq. 5.1. For the 16 sites lattice the 8 holes corresponding to quarter filling do not lead to a closed shell configuration. We need to choose $\mu = -2$ in order to obtain the proper limit for the Fermi sea. For the 50 sites lattice the 24 holes constitute a closed shell configuration, so there is some arbitrariness in the choice of μ . It has to be above the last filled and the first empty shell to yield the Fermi sea as a limit, *i.e.*, $-1.56 < \mu < -1$. For a finite D these values are not a strict limit. We use $\mu = -1.3$ and $\mu = -1.5$ and find that the energy does not depend significantly on μ ; as expected, the main variational parameter is the BCS gap D . For each value of J/t we determine the best variational energy according to the Rayleigh-Ritz principle, which leads to the lines labeled as “RR” in Fig. 5.2.

When we allow the generalized Lanczos operator \mathcal{A} (Eq. 5.2) to act on the wavefunction Eq. 5.1, we have 3 additional variational parameters α_1 , α_2 , and α_3 .⁶ Again we find the optimal variational parameters for each value of J/t and arrive at

⁵The limit $\Delta_{\mathbf{k}} \rightarrow \infty$ can be performed analytically. It leads to a slightly more complicated variant of the RVB determinant of section 2.7. This increases the complexity and the time requirement of the program, and we have not yet implemented this limit.

⁶ α_0 is determined by the normalization.

QUARTER FILLING — ENERGY

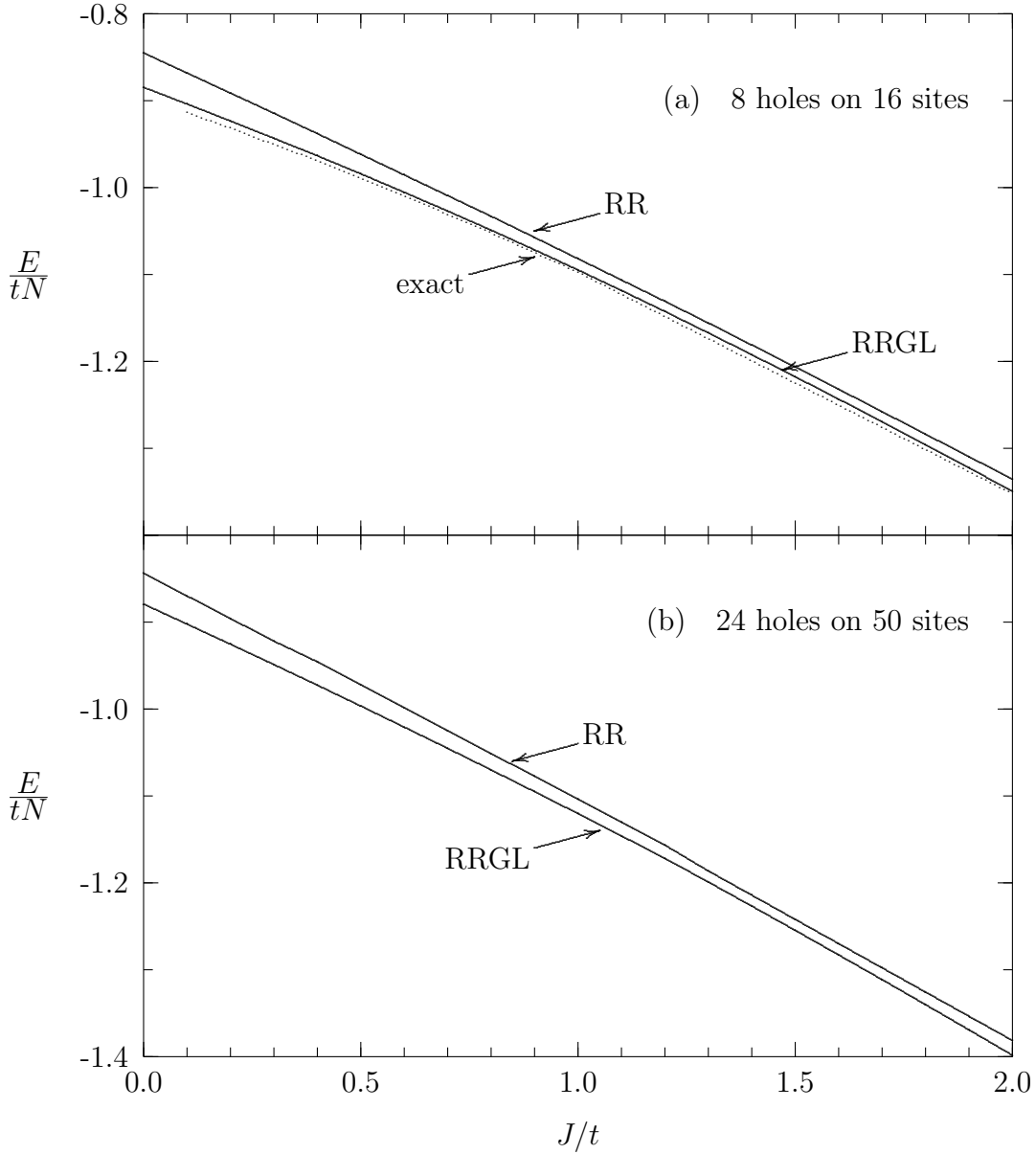


Figure 5.2: Energy per site in units of t as a function of coupling constant J/t for the t - J model at quarter filling. E_{RR} is the energy for the standard variational (Rayleigh-Ritz, RR) approach, whereas E_{RRGL} shows the energy after optimizing the short-range correlations with generalized Lanczos operators. The comparison with the exact results for 16 sites (dotted line) shows that generalized Lanczos operators lead to a considerable improvement. The statistical error is smaller than the line width.

QUARTER FILLING — VARIANCE

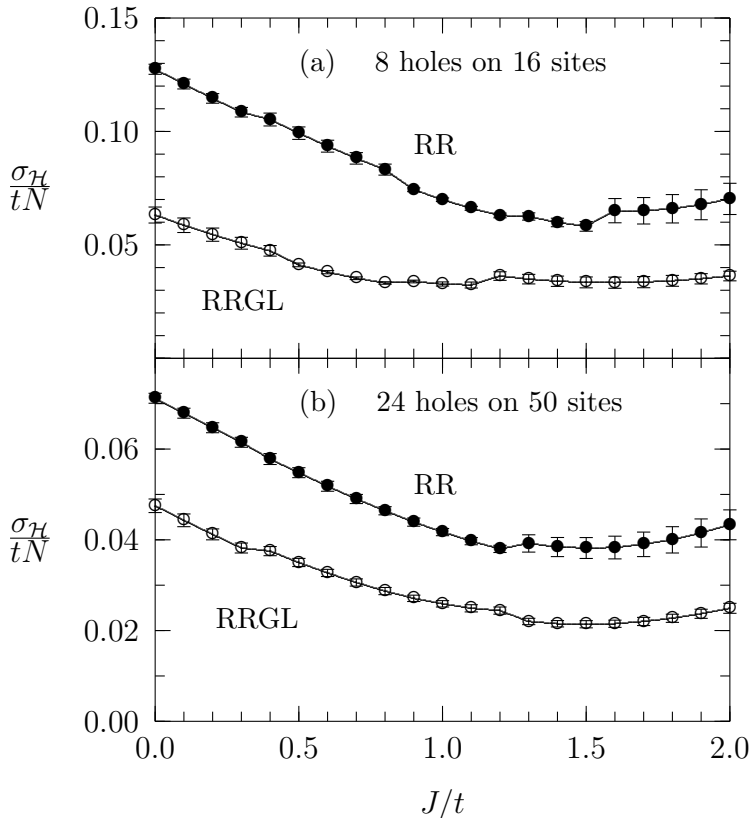


Figure 5.3: Variance as a function of coupling constant J/t . Shown is the standard deviation $\sigma_{\mathcal{H}}$ which is the square root of the variance. This value measures the width of the energy spectrum and indicates the quality of the wavefunction. RR and RRGL correspond to the same wavefunctions as for the energies.

the lines labeled with “RRGL” (Rayleigh-Ritz with generalized Lanczos operators). We compare our results with the exact groundstate energies from Ref. [105] and find that the generalized Lanczos iterations reduce the energy difference typically by a factor of 5. This means that the local correlations account for about 80% of the missing correlation energy. We therefore conclude that the combination of adjusting the long-range behavior with the parameter D in the wavefunction and the short-range behavior with the parameters α_i in the generalized Lanczos operators leads to a variational wavefunction which is a very good approximation to the groundstate. It should be noted that this improvement is possible despite the degeneracies caused by the open shell. For the closed shell of 24 holes on 50 sites we expect the results to be at least of the same quality.

In Fig. 5.3 we show the standard deviation $\sigma_{\mathcal{H}}$ of the Hamiltonian for the same optimized wavefunctions as for the energies in Fig. 5.2 before (“RR”) and after (“RRGL”) applying the generalized Lanczos operators. The standard deviation (or equivalently the variance $\sigma_{\mathcal{H}}^2$) is an indication of the quality of the wavefunction. It measures the deviation from an eigenstate as discussed in section 2.1. As we get closer to the groundstate we expect $\sigma_{\mathcal{H}}$ to converge to zero. Indeed we can see that $\sigma_{\mathcal{H}}$ is reduced typically by a factor of 2. Further we note that the wavefunctions on

the 50 sites already start with a slightly lower variance. As the standard deviations have been divided by the number of sites to account for the finite size scaling, this difference can be ascribed mostly to the fact that the 8 holes on 16 sites correspond to an open shell configuration. This again confirms the expectation that the closed shell configuration on the 50 sites lattice yields results which are at least as reliable as those for 16 sites.

The convergence to the groundstate can be seen even more clearly when using the relations Eqs. (2.4) and (2.5). As discussed in section 2.5 the energy should converge linearly with the variance $\sigma_{\mathcal{H}}^2$ towards the groundstate energy. In Fig. 5.4 we show the energy and variance for various different variational wavefunctions and a fixed value of $J/t = 1.0$. The points shown as \circ are obtained by standard variational Monte Carlo, each corresponding to a different choice of the gap parameter D . For the same wavefunctions we apply the generalized Lanczos operators Eq. (5.2) with individually optimized α_i parameters and arrive at the points shown as \diamond . We can see that the points form approximately a straight line. The improved wavefunctions clearly converge to the groundstate. This is a confirmation that the wavefunctions not only provide a good variational upper bound to the groundstate energy but also have a large overlap with the groundstate. This allows us to use the variational wavefunctions to calculate properties of the groundstate other than the energy.

We would like to point out that the typical variances for the 50 sites lattice are much smaller than those of the 16 sites lattice. To obtain the pair for 50 sites with a variance of around $0.01(tN)^2$ we had to choose a gap parameter of $D = 5t$ which also leads to an unfavorably high energy. All other points (also those of the 16 sites lattice) have a gap parameter $D \leq 1.0$. As mentioned above this can be explained as caused by the closed shell for the 50 sites as opposed to the open shell with the artificial degeneracy for the 16 sites at quarter filling.

In principle, one could perform an extrapolation to zero variance in order to obtain an estimate for the groundstate energy. However, such an extrapolation is not well controlled, *i.e.*, we cannot easily estimate the accuracy of such an extrapolation. Qualitatively, we can already see without an explicit extrapolation that the lowest variational state after the application of the generalized Lanczos operators is very close to the groundstate. Using this wavefunction instead of an extrapolation provides (a) a rigorous upper bound to the groundstate energy, and (b) allows the investigation of other observables, since the wavefunction is well defined.

This constitutes a considerable step towards the elimination of the main objection against any variational approach. A bias introduced through an inappropriate choice of the initial wavefunction would lead to points in the E vs. σ^2 diagram which move away from an excited eigenstate as the Lanczos iteration lowers the

QUARTER FILLING — CONVERGENCE

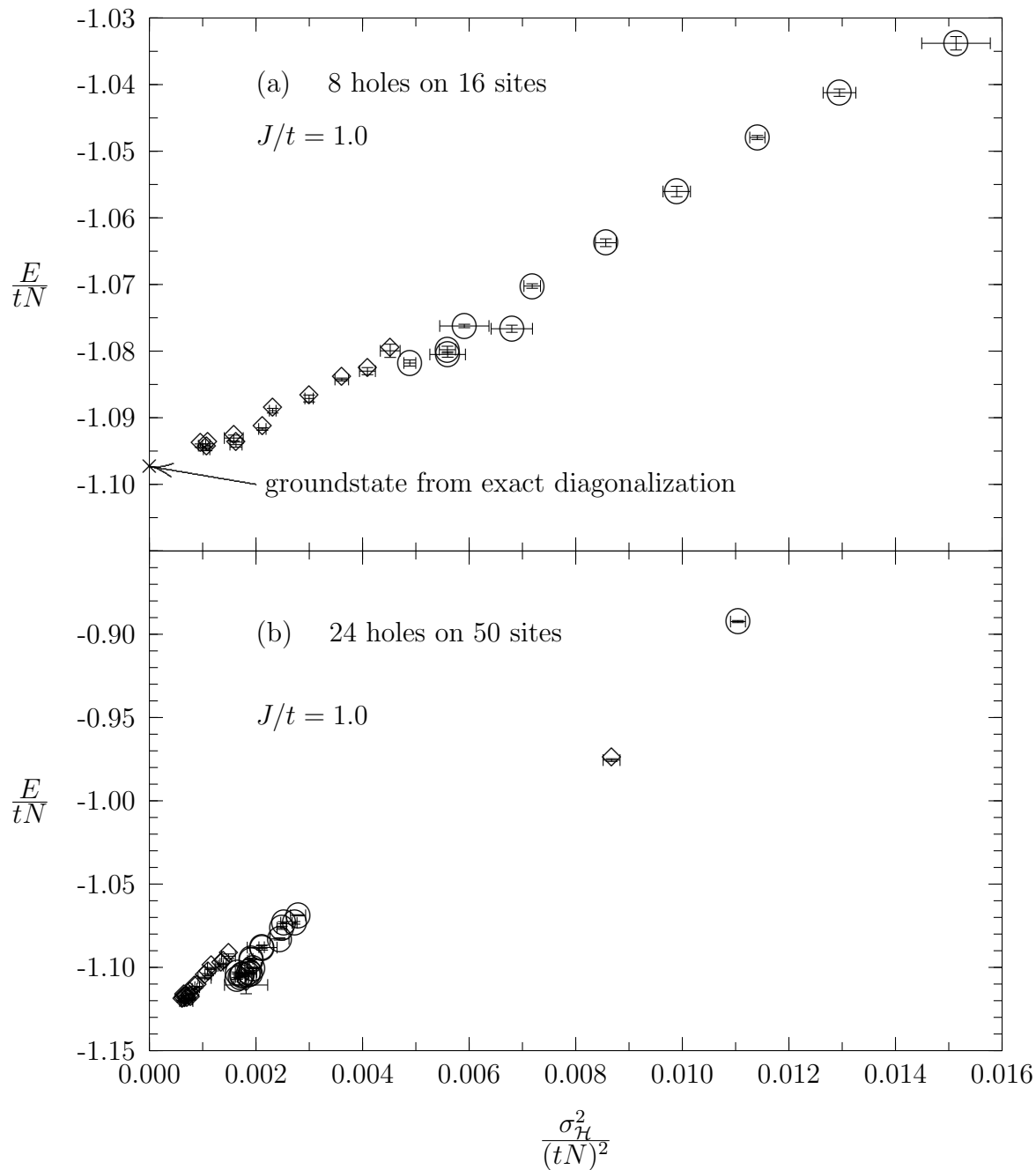


Figure 5.4: Energy and Variance for different variational wavefunctions before (\circ) and after (\diamond) the application of the generalized Lanczos operators. Near the groundstate we expect these points to lie close to a straight line. The exact result for 16 sites shows the success of the method. For 50 sites we obtain an analogous result with typically even smaller variances due to the closed shell configuration

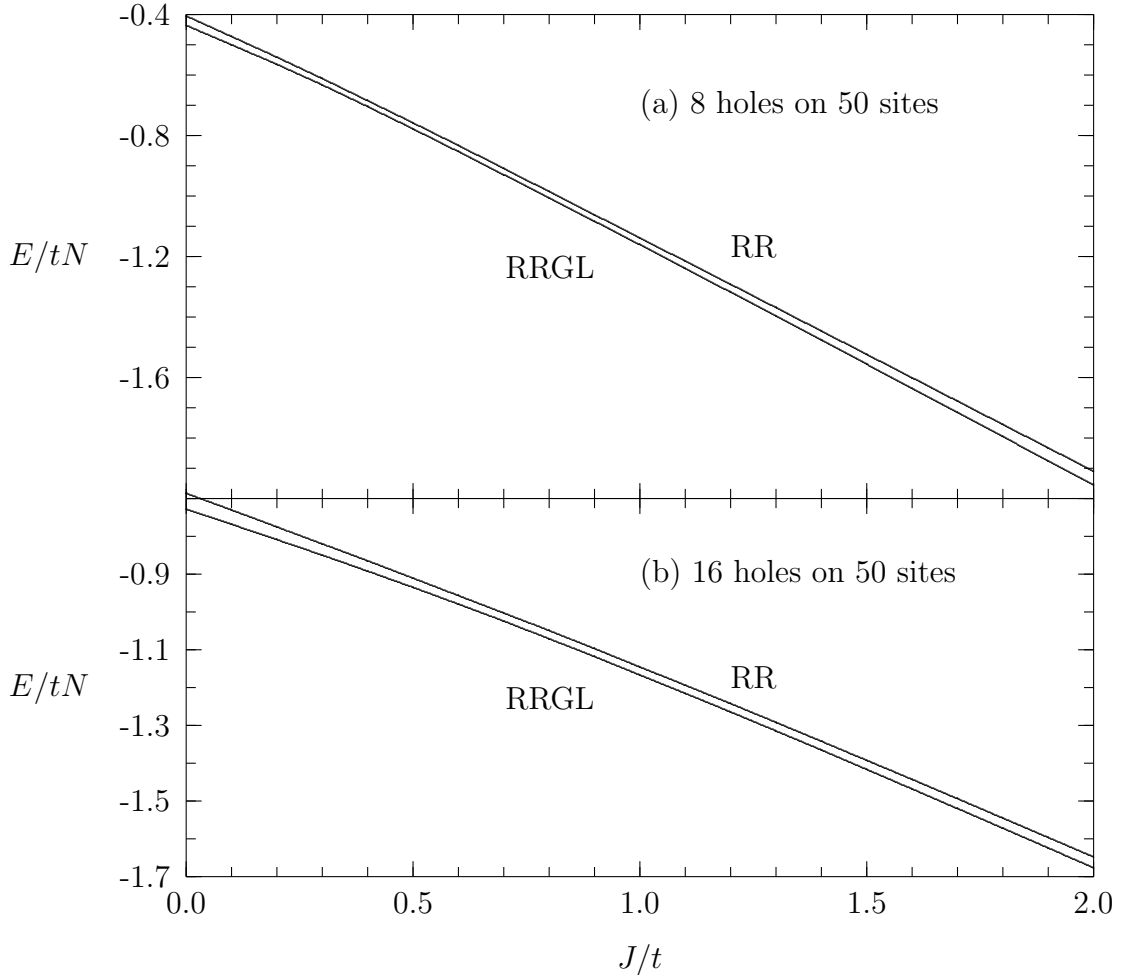


Figure 5.5: Energy per site in units of t as a function of the coupling constant J/t for the t - J model on a 50 sites lattice. (a) 8 holes, (b) 16 holes are both closed shells (*i.e.*, with minimal finite size effects). RR shows the standard variational energy (Rayleigh-Ritz) and RRGL shows the energy improved with generalized Lanczos operators.

energy or which would show an irregular scatter if too many excited state have a non-negligible weight. In conclusion we find that the use of the generalized Lanczos operators provides a powerful unbiased tool for a systematic improvement of variational wavefunctions.

5.1.2 Hole Dopings $\delta = 0.16$ and $\delta = 0.32$

The cases of 8 and 16 holes on the 50 sites lattice are investigated in analogy to the quarter filling case. Both of these fillings correspond to closed shells for the Fermi sea. This limit will therefore be well defined and there is no artificial degeneracy due to finite size effects. Because these are closed shells there is again some freedom

$\delta = 0.16$ AND $\delta = 0.32$ — CONVERGENCE

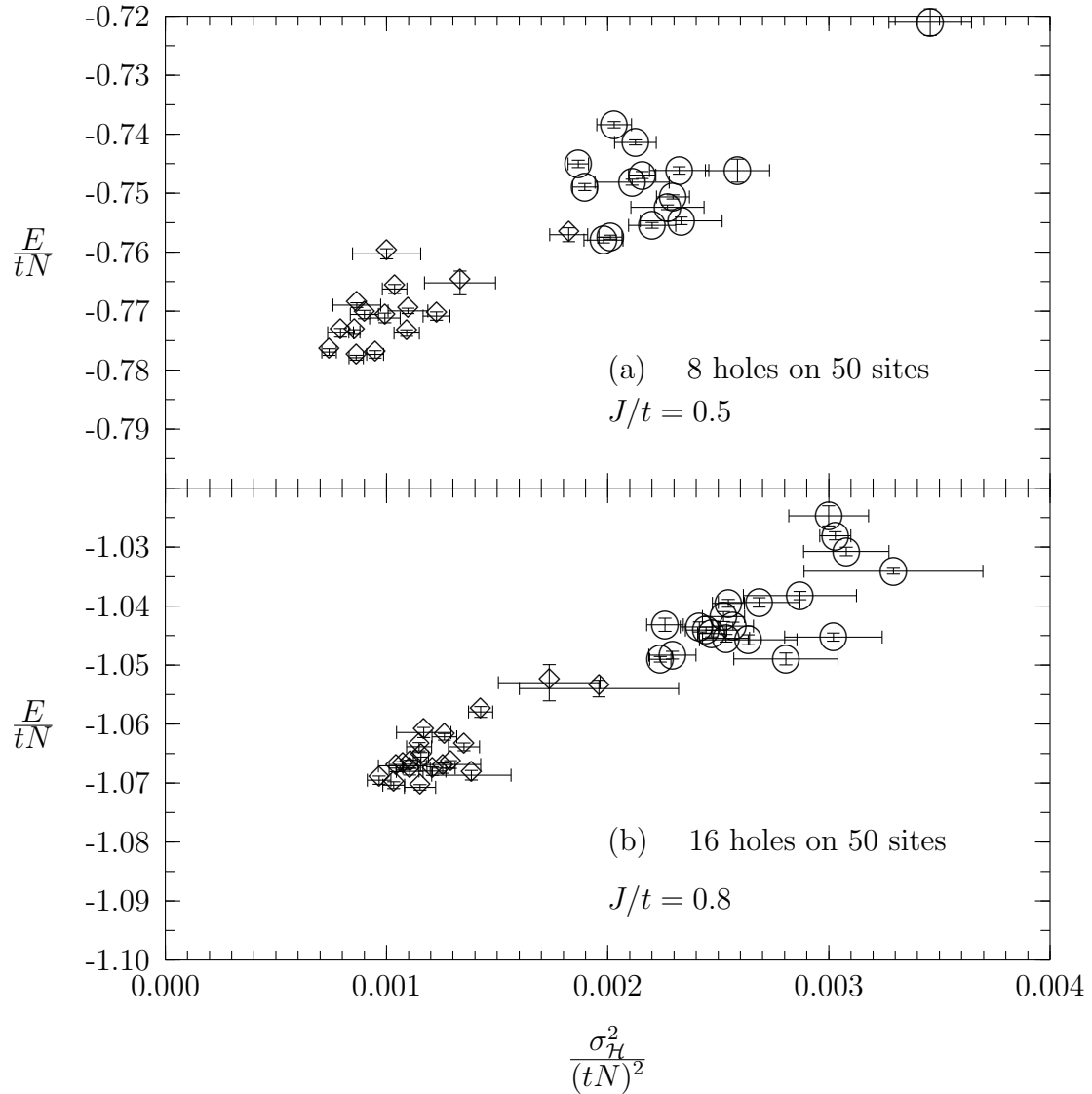


Figure 5.6: Test for convergence to the groundstate. The energy converges linearly as a function of σ^2 to the groundstate energy for wavefunctions which are close to the groundstate. For both fillings $\delta = 0.16$ (a) and $\delta = 0.32$ (b) we find a good convergence. The points \circ are obtained by standard variational Monte Carlo, while \diamond are optimized using the generalized Lanczos operators.

in the choice of μ in Eq. (5.1). To obtain the Fermi sea in the limit $D \rightarrow \infty$ we choose $\mu = -0.5$ for 8 holes on 50 sites and $\mu = -0.9$ for 16 holes on 50 sites.

Fig. 5.5 shows the energy for these two cases. Like for the case of quarter filling, we denote by “RR” the optimal energy we obtain for the standard variational Monte Carlo approach using the Rayleigh-Ritz principle for the wavefunction Eq. (5.1). The systematic improvement with the generalized Lanczos operators Eq. (5.2) yields the optimized energies labeled “RRGL”. The Lanczos iteration decreases the energy by amounts comparable to the quarter filling case.

In order to perform a qualitative test for the convergence to the groundstate, we use again the variance. Fig. 5.6 shows the energy and variance for different wavefunctions. The points \circ denote the values obtained for the standard variational wavefunctions, while the same wavefunctions yield the points \diamond when their short-range correlations are optimized using the generalized Lanczos operators. Here we show only the results for one value of J/t for each of the two cases, while for other values the behavior is qualitatively the same.⁷

5.2 Phase Separation

The wavefunction Eq. 5.1 describes a homogeneous electron distribution for all variational parameters. It cannot be used to model the phase separated region of the phase diagram. Furthermore, true phase separation only occurs in the thermodynamic limit. A finite but large enough system will show some density fluctuations indicative of phase separation. Because parts of the system belong to one or the other phase, we should expect a relatively large system to be necessary to show these density fluctuations.

Alternatively, we can imagine the *inhomogeneous* system to be composed of many smaller *homogeneous* systems of different densities. Whether the system exhibits phase separation is the result of an energy balance between two cases: (a) the large system is a mixture of subsystems of two different densities, or (b) all the subsystems have the same density, *i.e.*, the total system is homogeneous.

If the density of the total system is δ then a composition of subsystems with densities δ_1 and δ_2 with the same total density will have an energy

$$E_{composed}(\delta) = \frac{\delta_1 - \delta}{\delta_1 - \delta_2} E(\delta_1) + \frac{\delta - \delta_2}{\delta_1 - \delta_2} E(\delta_2) \quad (5.3)$$

This is a straight line connecting the energies $E(\delta_1)$ and $E(\delta_2)$. This energy has to be compared with $E(\delta)$ of the homogeneous system. If the composed system has a

⁷The particular values chosen here correspond to the region with finite superconducting long-range order as shown later in section 5.3.

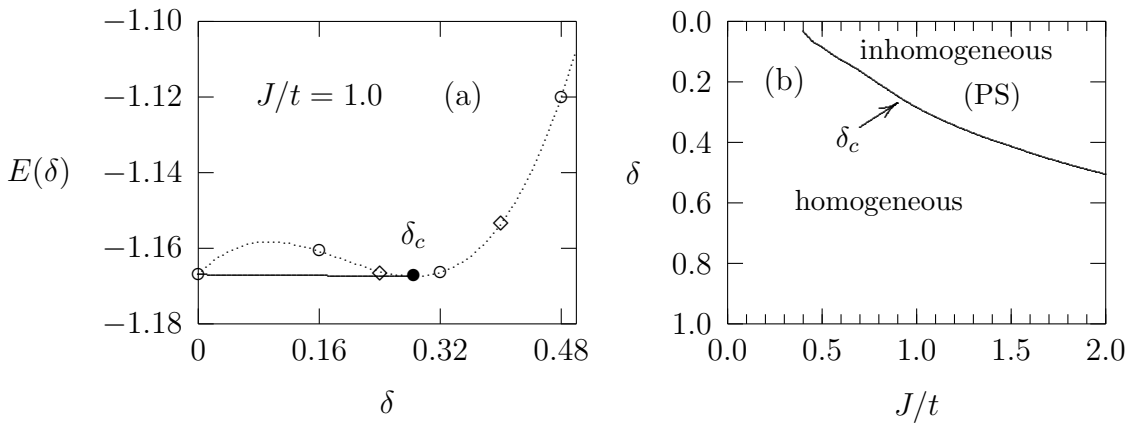


Figure 5.7: (a) Maxwell construction for $J/t = 1.0$. The straight line connecting $\delta = 0$ and δ_c lowers the energy. (b) phase separation line constructed from δ_c for different values of J/t .

lower energy than the homogeneous one, then the system will phase separate. The two densities which lead to the lowest energy determine the two components of the phase separated groundstate. This is known as the Maxwell construction (*e.g.*, see [106]).

To perform the Maxwell construction we need an expression for the energy of the homogeneous states as a function of the density δ . We can expect the energy of the *homogeneous* states to be a smooth function of the density and approximate it by a polynomial.

$$E(\delta) = \sum_i a_i \delta^i \quad (5.4)$$

Together with the Heisenberg energy for the half filled case we know the energies of the t - J model for each J/t for 4 densities, namely 0, 0.16, 0.32, and 0.48 corresponding to 0, 8, 16, and 24 holes on the 50 sites lattice. Each of these fillings corresponds to a closed shell configuration, so that we can expect the finite size effects to be minimal. The four values allow us to determine the coefficients of a third order polynomial as follows

$$\begin{pmatrix} a_0 \\ 0.16 a_1 \\ (0.16)^2 a_2 \\ (0.16)^3 a_3 \end{pmatrix} = \begin{pmatrix} 1 & 0 & 0 & 0 \\ -\frac{11}{6} & 3 & -\frac{3}{2} & \frac{1}{3} \\ 1 & -\frac{5}{2} & 2 & -\frac{1}{2} \\ -\frac{1}{6} & \frac{1}{2} & -\frac{1}{2} & \frac{1}{6} \end{pmatrix} \begin{pmatrix} E(0) \\ E(0.16) \\ E(0.32) \\ E(0.48) \end{pmatrix} \quad (5.5)$$

One of the two phases in the phase separated region corresponds to the density $\delta = 0$. The Maxwell construction finds a tangent to the polynomial starting from $E(0)$. This is shown in Fig. 5.7(a). The dotted line is the polynomial which runs through the data points shown as \circ . The solid line is the tangent which connects the point at $\delta = 0$ with a point at δ_c . For $0 < \delta < \delta_c$ a lower energy can be obtained by a mixture of the two phases. δ_c can be found from the polynomial coefficients

as

$$\delta_c = -\frac{a_2}{2a_3} \quad (5.6)$$

While in Fig. 5.7(a) we have chosen a fixed $J/t = 1.0$, we can repeat this procedure for each value of J/t . This results in the line shown in Fig. 5.7(b). Using the energies from the 50 sites lattice we can describe a much larger system composed of such smaller components. We can therefore expect that our result is a reasonable approximation of the thermodynamic limit. However, we only include homogeneous wavefunctions in our variational approach. We can therefore not exclude the possibility that inhomogeneous phases other than a phase separated state have a lower energy. Such phases include the formation of domain walls as conjectured by Prelovšek and Zotos[36]. We should regard the line shown in Fig. 5.7(b) as a lower bound for phase separation. Above this line some inhomogeneous state is expected. To find out about the details of this state we would need to modify the variational wavefunction or the generalized Lanczos operators to account for such inhomogeneous phases.

The knowledge of a fit to the energy $E(\delta)$ as a function of the density gives us the opportunity to test the influence of the finite size effects qualitatively. If we perform the same optimization procedure including the Lanczos iteration with the generalized operators for some open shell configurations, we arrive at the energies shown as \diamond in Fig. 5.7(a) for the fillings of 12 and 20 holes. We can see that these values are in good agreement with the dotted curve, which is fitted to the closed shell results (\circ). Therefore, we can expect the the finite size effects for the dopings in the range $0.16 < \delta < 0.48$ to be very small.

5.3 Superconducting Long-Range Order

To investigate the superconductivity we measure the pair-pair correlation function $C(R)$. This pair-pair correlation function is defined as

$$C(R) = (1/N) \sum_i \langle \Delta_i^\dagger \Delta_{i+R} \rangle \quad (5.7)$$

where for Δ_i we use a d-wave Cooper pair with short correlation length

$$\Delta_i = \frac{1}{2} \sum_{\sigma} c_{i,-\sigma} (c_{i+\hat{x},\sigma} + c_{i-\hat{x},\sigma} - c_{i+\hat{y},\sigma} - c_{i-\hat{y},\sigma}) \quad (5.8)$$

We find that for the 50 sites lattice $C(R)$ is flat for the larger distances indicating that the finite size effects are small. We can therefore take $C_{\infty} = C(R_{\max})$ as a measure for long-range order. In the standard variational approach C_{∞} is a mono-

tonic function of D and contains no additional information.⁸ However, we have seen for the Heisenberg case in section 4.3 that the Lanczos iteration may change the properties of the wavefunction so that the variational parameters in general have no more any particular significance for a property like the behavior of $C(R)$. It is hence important that we measure an observable explicitly and do not infer it from a variational parameter. In our case this means that we do not take D as a measure for the superconducting long-range order but only use C_∞ as a criterion.

With our new method of the generalized Lanczos iterations we can now test how the introduction of the short-range operators \mathcal{A} (Eq. (5.2)) in the wavefunction affects C_∞ . If we start with too much long-range order the operators \mathcal{A} will redistribute the weight in the correlation function and suppress C_∞ . On the other hand too small a value for C_∞ will be enhanced. If we start with the correct long-range order that corresponds to the groundstate, the operators \mathcal{A} will only affect the short range part of $C(R)$ and C_∞ will remain constant. In that case we have effectively separated the short- and long-range parts of the wavefunction.

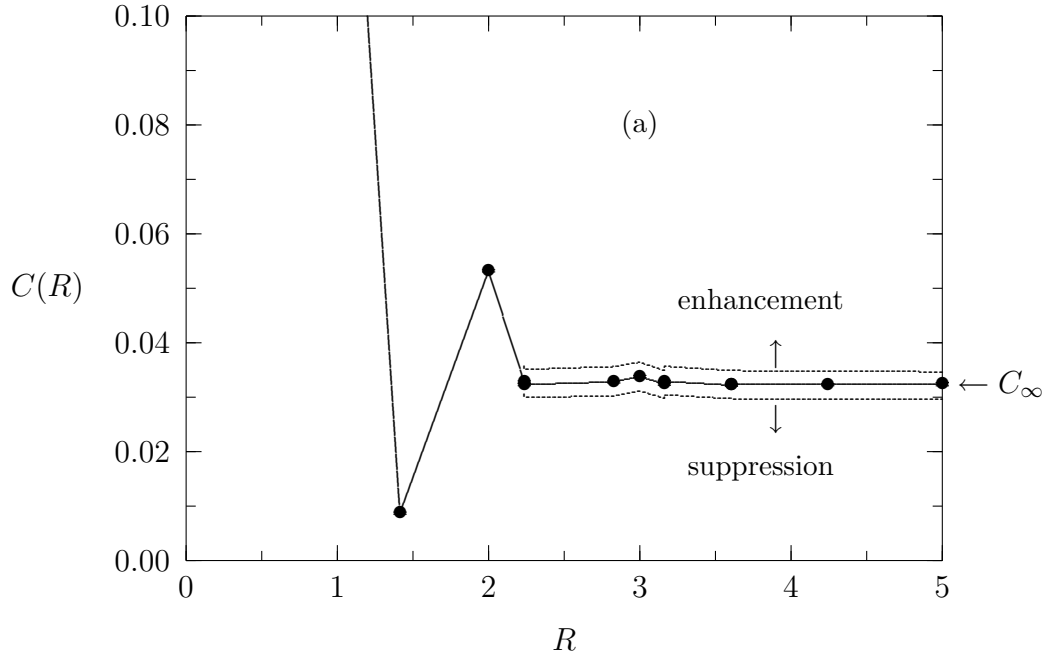
We will illustrate this for the case of 8 holes on 50 sites corresponding to a hole density of 0.16. In Fig. 5.8(a) we show $C(R)$ for one value of $D = 0.4t$ and $\mu = -0.8t$. The solid line corresponds to the RR-wavefunction. We can see that the long-range tail is well saturated. For $J < J_c$ the long-range correlations are suppressed, while for $J > J_c$ they are enhanced. This is shown by the dashed lines. For $D = 0.4t$ we find $J_c \approx 1.0t$. We can now combine the data obtained for different gap parameters D . In Fig. 5.8(b) we show C_∞ as a function of the coupling constant J/t . The solid line again corresponds to the RR-value while the dashed line shows the suppression and enhancement for the RRGL-values, *i.e.*, after the Lanczos iteration. The point where the solid and dashed lines cross is the value \tilde{C}_∞ which remains unchanged under iteration and we take this as the long-range order C_∞ of the groundstate. For other values of the variational parameter D we repeat the same procedure and obtain the points shown in Fig. 5.8(b). The error bars in J/t indicate the region where the suppression or enhancement is within one standard deviation. We can thus map out $\tilde{C}_\infty(J/t)$ for the groundstate. The extrapolation from small values of \tilde{C}_∞ to zero leads to an estimate of the critical J_s above which the system exhibits superconducting long-range order. For this particular hole doping of $\delta = 0.16$ we obtain $J_s = (0.39 \pm 0.03)t$.

The pair creation operator Δ_i (Eq. (5.8)) is a special case of the general pair creation operator

$$\Delta_i^F = \frac{1}{2} \sum_{\sigma, \tau} F(\tau) c_{i, -\sigma} c_{i+\tau, \sigma} \quad (5.9)$$

⁸The variational parameter μ also influences C_∞ to some extent, but for a fixed value of μ C_∞ is monotonic in D .

PAIR-PAIR CORRELATION



SUPERCONDUCTING LONG-RANGE ORDER

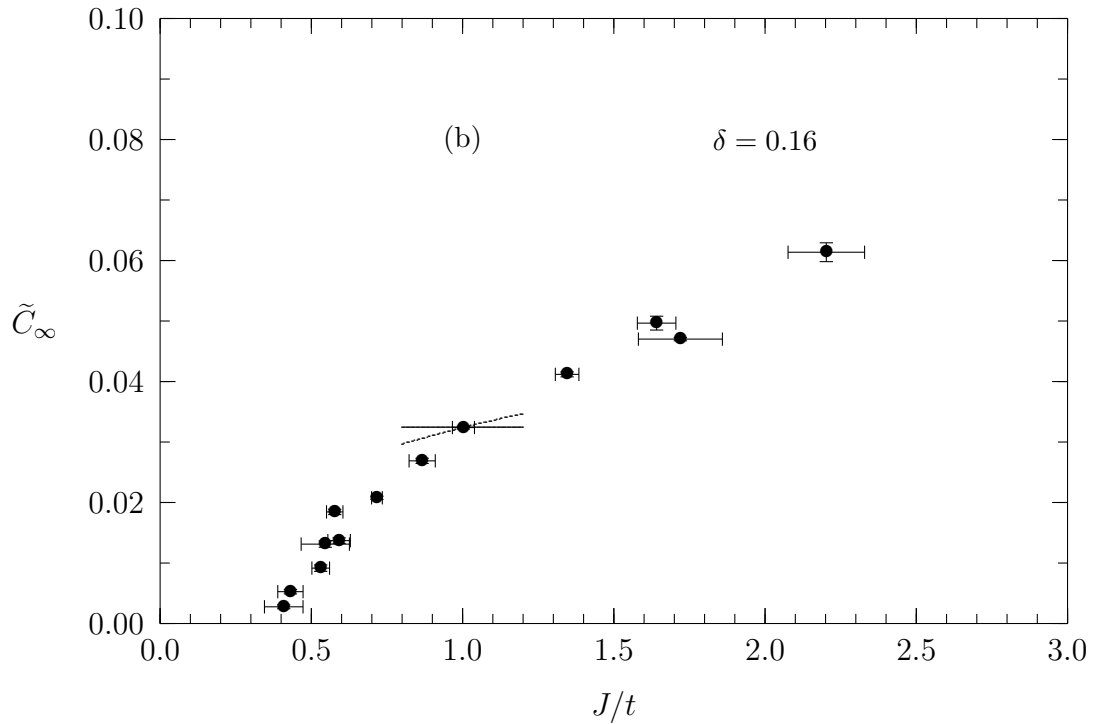


Figure 5.8: (a) d-wave pair-pair correlation function $C(R)$ as a function of distance for a hole density of 0.16 and a gap parameter $D = 0.4t$. The solid line corresponds to the raw RR wavefunction. The dashed lines show the long range correlation for the RRGL improvement for a value of $J > J_0$ and $J < J_0$ respectively. At the critical value J_0 the long-range correlation is unchanged from the RR ansatz. (b) long-range d-wave correlation C_∞ as a function of coupling constant J/t . The solid and dashed lines show C_∞ for the same gap parameter as in (a). For other variational parameters only the points $\tilde{C}_\infty(J/t)$ where C_∞ is unchanged are shown.

where $F(\tau)$ is the form factor of the cooper pair. With a Hamiltonian that has only nearest neighbor interactions it is reasonable to assume a form factor which is negligible for distances larger than one lattice spacing. This is also motivated by mean field approximations which lend themselves to the ansatz Eq. (5.1). Even if the actual cooper pairs of the groundstate should extend further, the overlap with the pair created by Δ_i will still be large. The long-range order \tilde{C}_∞ that we observe would then be slightly smaller than the true value but it still measures the existence of long-range order and can be used to determine onset of superconductivity in the phase diagram.

The size of the cooper pair also determines how large a system we have to use in order to have only negligible finite size effects for the superconducting phase. With a cooper pair that extends only to the nearest neighbor sites two pairs do not overlap anymore when they are more than two lattice spacings apart. This can be clearly seen in Fig. 5.8 — the large fluctuations of $C(R)$ die out at a distance of 2. Furthermore, the Lanczos iteration does not extend this range of the fluctuations. This is another confirmation that the cooper pairs in the groundstate have a short correlation length. It also shows that the largest available distance of 5 lattice spacings reflects the long-range behaviour very well.

This later condition is questionable for the 16 sites lattice, which was used for the exact diagonalization by Dagotto and Riera[40]. It's largest available distance is only $2\sqrt{2} \approx 2.83$. Nevertheless we can use the 16 sites lattice again to test the reliability of our approach by a comparison to the exact results. Fig. 5.9 shows the long distance pair-pair correlation \tilde{C}_∞ and the superconducting structure factor $S_{sc}(\mathbf{q} = 0)$ as a function of the coupling constant and compares them to the exact results. Neither of the two go to zero at any value of J/t , which is due to the rather small size of the system and does not indicate superconducting order. However, we can clearly reproduce the strong enhancement which was seen in the exact results at intermediate values of J/t . The sharp drop at the phase separation boundary cannot be found using the homogeneous ansatz Eq. (5.1) for the wavefunction. These results are again a confirmation that our new approach produces reliable results.

The convergence to the groundstate can also be seen in more detail if we plot the energy versus C_∞ . This is shown in Fig. 5.10 for 3 values of J/t . For each value of J/t the groundstate has a certain value for the energy and for C_∞ , *i.e.*, it corresponds to a point in the E versus C_∞ diagram. A variational wavefunction will always have a higher energy but can have an arbitrary value for C_∞ . The Lanczos iteration will take each starting wavefunction closer to the groundstate. This is indicated by the dotted lines in Fig. 5.10, which connect corresponding points before and after the Lanczos iteration. The 3 graphs illustrate the cases (a) $J/t = 0.2$ below the onset

16 SITES — SC CORRELATIONS

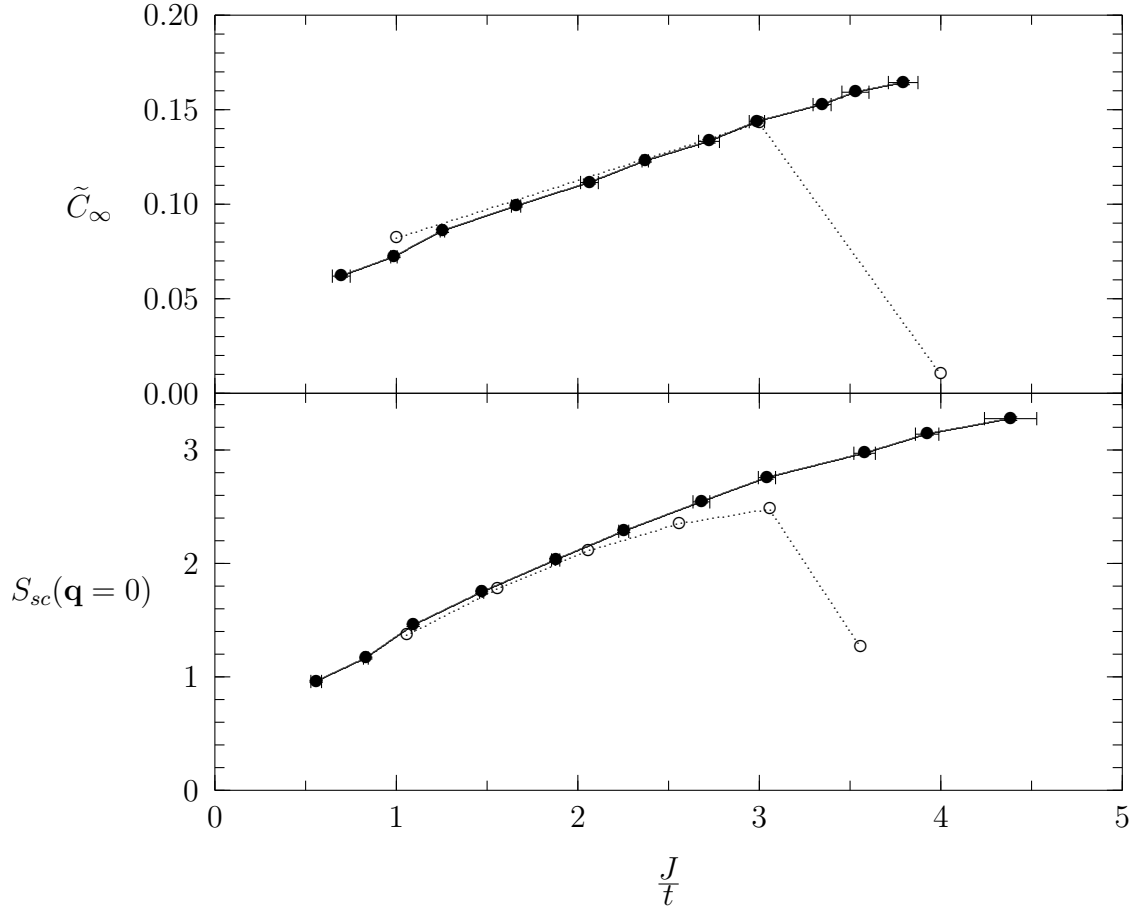


Figure 5.9: Comparison of our approach with exact diagonalization. Shown are the long-range pair-pair correlation C_∞ and the superconducting structure factor $S(\mathbf{q} = 0)$. Except for the phase separated region at high values of J/t our results (\bullet) reproduce the exact results (\circ) rather well.

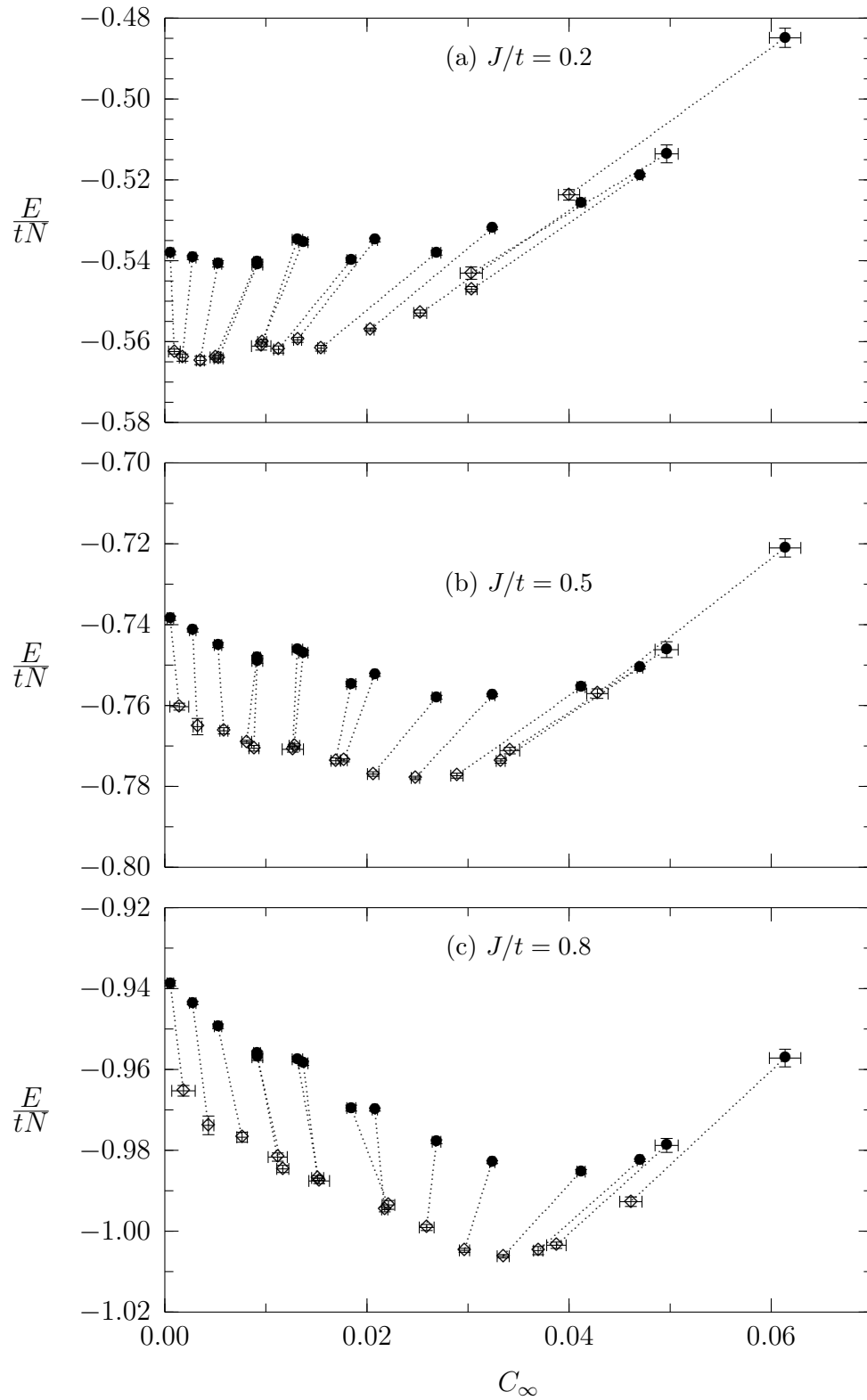


Figure 5.10: Energy versus long-range pair-pair correlation for a hole density of $\delta = 0.16$. Each pair of points connected by a dotted line corresponds to a different variational wavefunction before and after the Lanczos iteration. The energy is always lowered by the Lanczos iteration while C_∞ can be enhanced or suppressed.

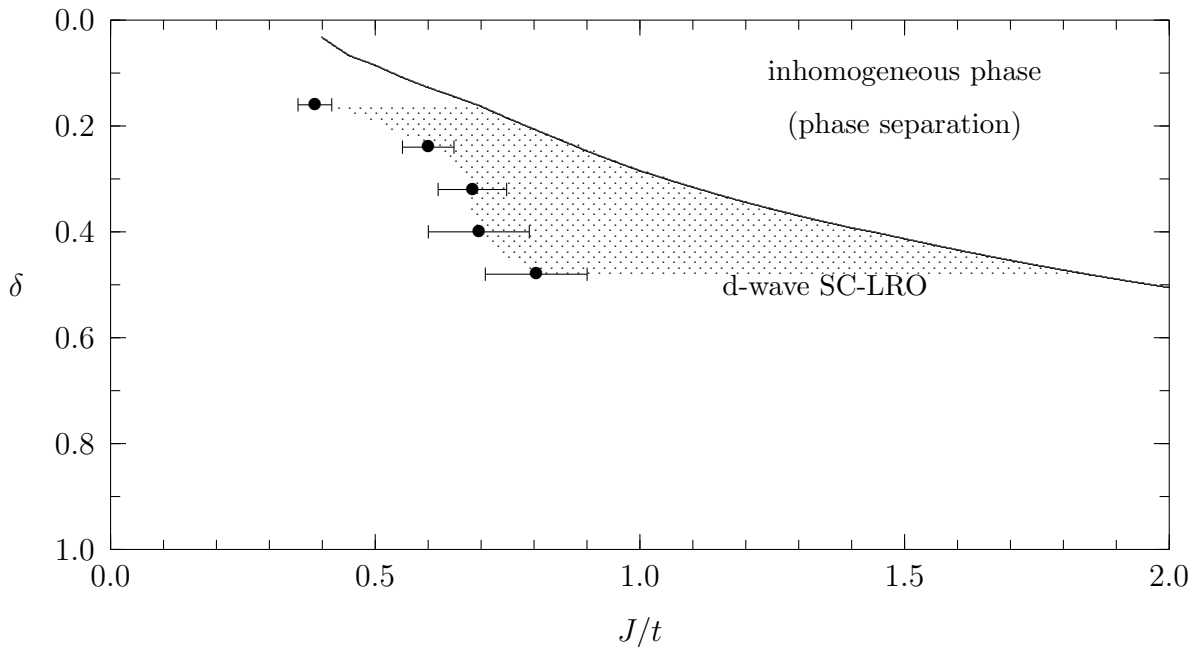


Figure 5.11: Phase diagram of the t - J model. The points denote the onset of d-wave superconducting long-range order as obtained by measuring the long-range pair-pair correlation of the groundstate \tilde{C}_∞ . Also shown is the phase separation line as obtained by the Maxwell construction. The shaded region shows a region d-wave superconductivity which we can follow down to a hole density of $\delta = 0.16$.

of long-range order, (b) $J/t = 0.5$ with a small but finite long-range order, and (c) $J/t = 0.8$ well within the superconducting region. Let us concentrate on case (b). From standard variational Monte Carlo alone, *i.e.*, taking only the upper points, one would estimate a value of $C_\infty \sim 0.03$ for the groundstate. Using the Lanczos iterations as just another way to construct a variational wavefunction would still yield $C_\infty \sim 0.025$. Only the criterion of the stability of the long-range order against the (short-ranged) Lanczos iteration as used above results in the value $\tilde{C}_\infty \approx 0.01$ which is clearly the most consistent limiting value for all the different variational wavefunctions. The standard variational approach overestimates the superconducting order.⁹ Even one Lanczos iteration would overestimate the superconducting order when only using the Rayleigh-Ritz criterion. With our new criterion however, we are able to eliminate the bias of the variational approach.

5.4 The Phase Diagram

With the same procedure that we used in the last section for a hole density of $\delta = 0.16$ we can determine the onset of superconductivity at other densities. Doing this we

⁹The variational wavefunctions are motivated by a mean field description and neglect quantum fluctuations.

arrive at the following values for J_s .

δ	J_s
0.16	0.39 ± 0.03
0.24	0.60 ± 0.05
0.32	0.68 ± 0.06
0.40	0.70 ± 0.10
0.48	0.80 ± 0.10

This allows us to construct the phase diagram Fig. 5.11. With the 50 sites lattice we can reliably determine the region of superconducting long-range order at hole densities in the range of $0.16 < \delta < 0.48$. We would like to emphasize that this system is large enough so that the finite size effects are negligible. This is qualitatively different from the results on small systems obtained by Dagotto and Riera[40] and Ohta *et al.*[41]. Their system is too small to detect any long-range order. At the largest distance available in the 16 and 18 sites lattices the cooper pairs are still very close to each other and their correlation has not yet reached the large distance value. This correlation will not be zero for the whole range of coupling constants J/t and cannot be used to determine the onset of superconductivity but only be taken as an indication of where the superconducting correlations are enhanced. Similarly, the static structure factor, which is the integral of the correlation function, is dominated by the short distances and has the same problems. This situation is quite different on the 50 sites lattice. The correlation function has clearly saturated at its large distance value and is a reliable measure for the long-range order. This allows us to determine the transition to a phase with superconducting long-range order.

Beyond the solid line in the phase diagram, in the region labeled “inhomogeneous phase”, our variational ansatz is not able to model the groundstate appropriately as a mixture of two phases leads to a lower energy. From our data we are not able to determine the nature of this groundstate. Depending on the coupling constant we can expect different types states ranging from the formation of domain walls up to true phase separation to occur. We can therefore conclude that the superconductivity extends at least up to the solid line, *i.e.*, in the shaded region of the phase diagram Fig. 5.11.

Chapter 6

Conclusions

We have shown in this thesis that our new approach of using generalized Lanczos operator provides a powerful unbiased way to systematically improve the variational Monte Carlo method. While it provides more reliable information than just an upper bound to the energy, it retains many of the advantages of a variational approach and even improves them.

- The systems that can be investigated are only slightly smaller than for the standard variational Monte Carlo, and they are certainly much larger than those available for exact diagonalizations.
- As the wavefunction is explicitly given it is possible to investigate specific instabilities like the formation of a BCS condensate or the formation of antiferromagnetic long-range order. Using the generalized Lanczos operators allows us to specify the nature of the variational state even more precisely.
- The systematic unbiased improvement obtained by the generalized Lanczos iteration provides a good criterion to judge how closely the variational wavefunction models the groundstate. This information is obtained by comparing both the energy *and* the variance before and after the iteration.

The results on the t - J model show that our method is able to produce non-trivial results which are comparable to those obtained by exact diagonalization. In extension to exact diagonalization we are able to investigate large enough systems that allow us find a phase transition to long-range order.

The success of our method originates mainly in the flexibility with which the wavefunctions and generalized Lanczos operators can be chosen. In the case of the t - J model we were able to address the short- and long-range behavior of the system separately. This feature can also be used in more general problems. Any Hamiltonian for which we know a reasonably good variational wavefunction can be investigated further using our approach. The Hamiltonian itself is enough to perform a Lanczos

iteration and its form often may suggest generalizations. Furthermore, even if for such a system it is not clear what a good choice for a variational ansatz would be, then the (generalized) Lanczos iteration provides a good criterion to judge different choices. Our method should therefore be viewed as a general tool used to improve a variational Monte Carlo treatment.

Bibliography

- [1] P. C. Hohenberg, Phys. Rev. **158**, 383 (1967).
- [2] J. M. Kosterlitz and D. J. Thouless, J. Phys. C **6**, 1181 (1973).
- [3] B. I. Halperin and D. R. Nelson, J. Low. Temp. Phys. **36**, 599 (1979).
- [4] N. D. Mermin and H. Wagner, Phys. Rev. Lett. **17**, 1133 (1966).
- [5] E. Dagotto, Rev. Mod. Phys. , in press.
- [6] A. P. Kampf, Magnetic correlations in high temperature superconductivity, Review article for Physics Reports, 1994.
- [7] W. Brenig, Aspects of electron correlations in the cuprate superconductors, submitted to Physics Reports.
- [8] P. Fulde, *Electron Correlations in Molecules and Solids*, volume 100 of *Solid-State Sciences*, Springer-Verlag, Berlin, 2nd edition, 1993.
- [9] M. S. Hybertsen, M. Schlüter, and N. E. Christensen, Phys. Rev. B **399**, 9028 (1989).
- [10] N. Nücker et al., Z. Phys. B **67**, 9 (1987).
- [11] F. C. Zhang and T. M. Rice, Phys. Rev. B **37**, 3759 (1988).
- [12] M. S. Hybertsen et al., Phys. Rev. B **41**, 11068 (1990).
- [13] J. Hubbard, Proc. Roy. Soc. (London), Ser. A **276**, 238 (1963).
- [14] J. Hubbard, Proc. Roy. Soc. (London), Ser. A **281**, 401 (1964).
- [15] S. Chakravarty, *High-Temperature Superconductivity*, Addison-Wesley, 1990.
- [16] R. J. Birgeneau, Am. J. Phys. **58**, 28 (1990).
- [17] B. Keimer et al., Phys. Rev. B **46**, 14034 (1992).

- [18] R. J. Birgeneau et al., Phys. Rev. B **38**, 6614 (1988).
- [19] T. R. Thurston et al., Phys. Rev. B **40**, 4585 (1989).
- [20] G. Shirane et al., Phys. Rev. Lett. **63**, 330 (1989).
- [21] Rossat-Minod, Physica B **163**, 4 (1990).
- [22] G. Shirane et al., Phys. Rev. B **41**, 6547 (1990).
- [23] S. M. Hayden et al., Phys. Rev. Lett. **66**, 821 (1991).
- [24] S. W. Cheong et al., Phys. Rev. Lett. **67**, 1791 (1991).
- [25] G. Aeppli, Lecture notes for E. Fermi Summer School, Varenna, Italy, 1992.
- [26] T. K. Lee and S. Feng, Phys. Rev. B **38**, 11809 (1988).
- [27] T. Giamarchi and C. Lhuillier, Phys. Rev. B **43**, 12943 (1991).
- [28] R. R. P. Singh and R. L. Glenister, Phys. Rev. B **46**, 11871 (1992).
- [29] Y. Nagaoka, Phys. Rev. **147**, 392 (1966).
- [30] W. O. Putikka, M. U. Luchini, and M. Ogata, Phys. Rev. Lett. **69**, 2288 (1992).
- [31] D. Poilblanc, Phys. Rev. B **45**, 10775 (1992).
- [32] V. J. Emery, S. A. Kivelson, and H. Q. Lin, Phys. Rev. Lett. **64**, 475 (1990).
- [33] M. Ogata et al., Phys. Rev. Lett. **66**, 2388 (1991).
- [34] W. O. Putikka, M. U. Luchini, and T. M. Rice, Phys. Rev. Lett. **68**, 538 (1992).
- [35] P. Prelovšek, J. Bonča, and I. Sega, Generalized t - j models on a chain as a substitute for planar systems, in *Physica C*, volume 185–189, page 1499, Kanazawa, Japan.
- [36] P. Prelovsek and X. Zotos, Phys. Rev. B **47**, 5984 (1993).
- [37] M. Imada and Y. Hatsugai, J. Phys. Soc. Jpn. **58**, 3752 (1989).
- [38] M. Imada, J. Phys. Soc. Jpn. **60**, 2740 (1991).
- [39] A. Moreo, Phys. Rev. B **45**, 5059 (1992).

- [40] E. Dagotto and J. Riera, Phys. Rev. Lett. **70**, 682 (1993).
- [41] Y. Ohta et al., preprint cond-mat/9403076.
- [42] P. Monthoux and D. J. Scalapino, Phys. Rev. Lett. **72**, 1874 (1994).
- [43] H. Yokoyama and H. Shiba, J. Phys. Soc. Jpn. **57**, 2483 (1988).
- [44] G. J. Chen et al., Phys. Rev. B **42**, 2662 (1990).
- [45] Q. P. Li, B. E. C. Koltenbah, and R. Joynt, Phys. Rev. B **48**, 437 (1993).
- [46] Y. C. Chen and T. K. Lee, to appear in Z. Phys. B.
- [47] Y. C. Chen et al., preprint cond-mat/9403037.
- [48] Y. C. Chen and T. K. Lee, preprint cond-mat/9404095.
- [49] C. S. Hellberg and E. J. Mele, Phys. Rev. Lett. **67**, 2080 (1991).
- [50] R. Valentí and C. Gros, Phys. Rev. Lett. **68**, 2402 (1992).
- [51] W. L. McMillan, Phys. Rev. **138**, A442 (1965).
- [52] D. Ceperley, G. V. Chester, and M. H. Kalos, Phys. Rev. B **16**, 3081 (1977).
- [53] G. Baym, *Lectures on Quantum Mechanics*, Benjamin/Cummings, Menlo Park, CA, 3rd printing, with corrections edition, 1974.
- [54] C. Gros, Phys. Rev. B **42**, 6835 (1990).
- [55] C. Lanczos, J. Res. Nat. Bur. Stand. **45**, 255 (1950).
- [56] R. Haydock, The Recursive Solution of the Schrödinger Equation, in *Solid State Physics*, volume 35, pages 215–294, Academic Press, 1980.
- [57] W. H. Press et al., *Numerical Recipes in C*, Cambridge University Press, Cambridge, 2nd edition, 1992.
- [58] J. H. Wilkinson and C. Reinsch, *Handbook for Automatic Computation*, Springer-Verlag, 1971.
- [59] F. S. Acton, *Numerical Methods That Work*, Harper and Row, New York, 2nd edition edition, 1990.
- [60] B. N. Parlett, *The Symmetric Eigenvalue Problem*, Prentice-Hall Series in Computational Mathematics, 1980.

- [61] Y. C. Chen and T. K. Lee, Phys. Rev. B **47**, 11548 (1993).
- [62] W.-K. Tung, *Group Theory in Physics*, World Scientific, Philadelphia, 1985.
- [63] J. P. Elliott and P. G. Dawber, *Symmetry in Physics*, MacMillan, London, 1979.
- [64] E. Dagotto and J. R. Schrieffer, Phys. Rev. B **43**, 8705 (1991).
- [65] C. Gros, Annals of Physics **189**, 53 (1989).
- [66] K. Binder and D. W. Heermann, *Monte Carlo Simulation in Statistical Physics*, volume 80 of *Springer Series in Solid-State Sciences*, Springer-Verlag, Berlin, 1988.
- [67] N. Metropolis et al., J. Chem. Phys. **21**, 1087 (1953).
- [68] H. Gränicher, Grundlagen physikalischer Messungen, ETH lecture notes, 1984.
- [69] *Condor Distributed Batch System*, by Michael Litzkow <mike@cs.wisc.edu>, University of Wisconsin, Madison, available by anonymous ftp on the internet from ftp.cs.wisc.edu.
- [70] Optimizing GNU C++ compiler from the Free Software Foundation, Cambridge, Massachusetts, available by anonymous ftp from prep.ai.mit.edu.
- [71] H. A. Bethe, Z. Phys. **71**, 205 (1931).
- [72] F. Dyson, E. H. Lieb, and B. Simon, J. Stat. Phys. **18**, 335 (1978).
- [73] T. Kennedy, E. H. Lieb, and B. S. Shastry, J. Stat. Phys. **53**, 1019 (1988).
- [74] E. J. Neves and J. F. Perez, Phys. Lett. A **114A**, 331 (1986).
- [75] K. Kubo and T. Kishi, Phys. Rev. Lett. **61**, 2585 (1988).
- [76] K. Kubo, Phys. Rev. Lett. **61**, 110 (1988).
- [77] W. Marshall, Proc. Roy. Soc. (London), Ser. A **232**, 48 (1955).
- [78] W. Marshall, Proc. Roy. Soc. (London), Ser. A **232**, 69 (1955).
- [79] J. Oitmaa and D. D. Betts, Can. J. Phys. **56**, 897 (1978).
- [80] S. Tang and J. E. Hirsch, Phys. Rev. B **39**, 4548 (1989).
- [81] S. Tang and H. Q. Lin, Phys. Rev. B **38**, 6863 (1988).

- [82] N. Trivedi and D. M. Ceperley, Phys. Rev. B **40**, 2737 (1989).
- [83] J. Carlson, Phys. Rev. B **40**, 846 (1989).
- [84] P. W. Anderson, Phys. Rev. **86**, 694 (1952).
- [85] R. Kubo, Phys. Rev. **87**, 568 (1952).
- [86] T. Oguchi, Phys. Rev. **117**, 117 (1960).
- [87] H. L. Davis, Phys. Rev. **120**, 789 (1960).
- [88] M. Parrinello and T. Arai, Phys. Rev. B **10**, 265 (1974).
- [89] D. Huse, Phys. Rev. B **37**, 2380 (1988).
- [90] R. R. P. Singh, Phys. Rev. B **39**, 9760 (1989).
- [91] H. Yokoyama and H. Shiba, J. Phys. Soc. Jpn. **56**, 3582 (1987).
- [92] H. Yokoyama and H. Shiba, J. Phys. Soc. Jpn. **56**, 3570 (1987).
- [93] D. A. Huse and V. Elser, Phys. Rev. Lett. **60**, 2531 (1988).
- [94] Z. Liu and E. Manousakis, Phys. Rev. B **40**, 11437 (1989).
- [95] R. Shankar and G. Murthy, Phys. Lett. A **137**, 165 (1989).
- [96] E. Manousakis, Rev. Mod. Phys. **63**, 1 (1991).
- [97] T. Holstein and H. Primakoff, Phys. Rev. **58**, 1098 (1940).
- [98] S. Liang, B. Doucot, and P. W. Anderson, Phys. Rev. Lett. **61**, 365 (1988).
- [99] E. S. Heeb and T. M. Rice, Z. Phys. B **90**, 73 (1993).
- [100] N. Trivedi and D. M. Ceperley, Phys. Rev. B **41**, 4552 (1990).
- [101] J. D. Jorgensen et al., Phys. Rev. B **38**, 11337 (1988).
- [102] D. R. Harshman et al., Phys. Rev. Lett. **63**, 1187 (1989).
- [103] P. C. Hammel et al., Phys. Rev. B **42**, 6781 (1990).
- [104] A. J. Millis, H. Monien, and D. Pines, Phys. Rev. B **42**, 167 (1990).
- [105] E. Dagotto et al., Phys. Rev. B **45**, 10107 (1992).
- [106] K. Huang, *Statistical Mechanics*, John Wiley & Sons, New York, 1987.

Curriculum Vitae

7. Dec. 1964 Born in Glarus, Switzerland
- 1971 – 1977 Primary school in Rebstein SG, Switzerland
- 1977 – 1979 Secondary school in Altstätten SG, Switzerland
- 1979 – 1983 Mittelschule, Kantonsschule Heerbrugg SG, Switzerland
- 1983 Maturität Typus C, Kantonsschule Heerbrugg SG
- 1984 – 1989 Study of Physics at the Swiss Federal Institute of Technology (ETH) in Zürich
- 1989 Diploma thesis on “*Spezifische Wärme von intermetallischen Verbindungen bei tiefen Temperaturen*” at the Laboratorium für Festkörperphysik at the ETH Zürich under the supervision of Prof. Dr. H. R. Ott
- 1/1/1990 – today Graduate student at the Institute for Theoretical Physics of the Swiss Federal Institute of Technology (ETH) in Zürich, Switzerland